Cell Reports

Article

Stem-like progenitor and terminally differentiated T_{FH}-like CD4$^+$ T cell exhaustion in the tumor microenvironment

Graphical abstract

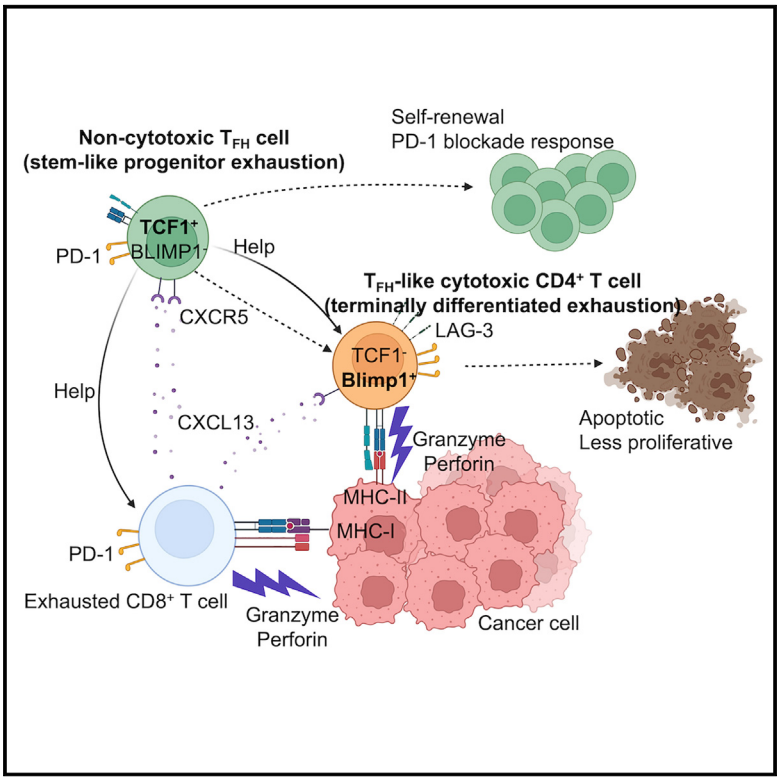

Highlights

- CXCL13 produced by exhausted CD8$^+$ T cells in the TME recruits T_{FH} cells
- A part of T_{FH} cells has cytotoxicity against MHC-II-expressing tumors
- The BLIMP1/TCF1 axis determines the differentiation of cytotoxicity
- T_{FH}-like CD4$^+$ T cells in the TME have features similar to exhausted CD8$^+$ T cells

Authors

Wenhao Zhou, Shusuke Kawashima, Takamasa Ishino, ..., Takashi Inozume, Joji Nagasaki, Yosuke Togashi

Correspondence

george.nagasaki.1985@gmail.com (J.N.), ytogashi1584@gmail.com (Y.T.)

In brief

Zhou et al. demonstrate that CXCL13 produced by cancer-specific exhausted CD8$^+$ T cells in the TME recruits T_{FH} cells, a part of which exhibits cytotoxicity. The BLIMP1/TCF1 axis determines the nature of these T_{FH} cells, which resembles the concept of stem-like progenitor/terminally differentiated exhaustion in CD8$^+$ T cells.

Zhou et al., 2024, Cell Reports *43*, 113797
February 27, 2024
https://doi.org/10.1016/j.celrep.2024.113797

CellPress

Cell Reports

CellPress
OPEN ACCESS

Article

Stem-like progenitor and terminally differentiated T_{FH}-like $CD4^+$ T cell exhaustion in the tumor microenvironment

Wenhao Zhou,[1,2,3,12] Shusuke Kawashima,[4,5,12] Takamasa Ishino,[1,5,6] Katsushige Kawase,[5,7] Youki Ueda,[1] Kazuo Yamashita,[8] Tomofumi Watanabe,[1,9] Masahito Kawazu,[5] Hiromichi Dansako,[1] Yutaka Suzuki,[10] Hiroyoshi Nishikawa,[2,11] Takashi Inozume,[4,5] Joji Nagasaki,[1,5,*] and Yosuke Togashi[1,5,11,13,*]

[1]Department of Tumor Microenvironment, Okayama University Graduate School of Medicine, Dentistry and Pharmaceutical Sciences, Okayama 700-8558, Japan
[2]Department of Immunology, Nagoya University Graduate School of Medicine, Nagoya 466-8550, Japan
[3]Department of Urology Surgery, Affiliated Hospital of North Sichuan Medical College, Nanchong, China
[4]Department of Dermatology, Chiba University Graduate School of Medicine, Chiba 260-8670, Japan
[5]Chiba Cancer Center, Research Institute, Division of Cell Therapy, Chiba 260-8717, Japan
[6]Department of Gastroenterology, Graduate School of Medicine, Chiba University, Chiba 260-8670, Japan
[7]Department of Otorhinolaryngology/Head & Neck Surgery, Graduate School of Medicine, Chiba University, Chiba 260-8670, Japan
[8]KOTAI Biotechnologies, Inc. Osaka 565-0871, Japan
[9]Department of Urology, Okayama University Graduate School of Medicine, Dentistry and Pharmaceutical Sciences, Okayama 700-0932, Japan
[10]Department of Computational Biology and Medical Sciences, Graduate School of Frontier Sciences, The University of Tokyo, Kashiwa, Kashiwa 277-8568, Japan
[11]Division of Cancer Immunology, National Cancer Center, Research Institute/Exploratory Oncology Research and Clinical Trial Center (EPOC), Tokyo 104-0045, Kashiwa 277-8577, Japan
[12]These authors contributed equally
[13]Lead contact
*Correspondence: george.nagasaki.1985@gmail.com (J.N.), ytogashi1584@gmail.com (Y.T.)
https://doi.org/10.1016/j.celrep.2024.113797

SUMMARY

Immune checkpoint inhibitors exert clinical efficacy against various types of cancer through reinvigoration of exhausted $CD8^+$ T cells that attack cancer cells directly in the tumor microenvironment (TME). Using single-cell sequencing and mouse models, we show that *CXCL13*, highly expressed in tumor-infiltrating exhausted $CD8^+$ T cells, induces $CD4^+$ follicular helper T (T_{FH}) cell infiltration, contributing to anti-tumor immunity. Furthermore, a part of the T_{FH} cells in the TME exhibits cytotoxicity and directly attacks major histocompatibility complex-II-expressing tumors. T_{FH}-like cytotoxic $CD4^+$ T cells have high LAG-3/BLIMP1 and low TCF1 expression without self-renewal ability, whereas non-cytotoxic T_{FH} cells express low LAG-3/BLIMP1 and high TCF1 with self-renewal ability, closely resembling the relationship between terminally differentiated and stem-like progenitor exhaustion in $CD8^+$ T cells, respectively. Our findings provide deep insights into T_{FH}-like $CD4^+$ T cell exhaustion with helper progenitor and cytotoxic differentiated functions, mediating anti-tumor immunity orchestrally with $CD8^+$ T cells.

INTRODUCTION

The immune system comprises a sophisticated machinery that protects the host from various infectious diseases and cancer. Cancer immunotherapies, especially immune checkpoint inhibitors (ICIs), act by reinvigoration of effector $CD8^+$ T cells in the tumor microenvironment (TME); they have revolutionized cancer therapy across multiple types of cancer.[1–4] Although durable response and favorable clinical prognosis have been reported in a fraction of patients, the low response rate, severe immune-related adverse events, and acquired resistance limit the use of ICIs.[1–4] Therefore, predictive biomarkers and further understanding of anti-tumor immune responses, including interactions in the TME, are necessary for boosting immunotherapy.

Follicular helper T cells (T_{FH} cells) are a subgroup of $CD4^+$ T cells characterized by the expression of programmed cell death protein 1 (PD-1) and CXCR5, along with the transcription factor BCL6.[5,6] A canonical T_{FH} cell differentiation usually occurs in secondary lymphoid organs, where naive $CD4^+$ T cells are primed by peptide-major histocompatibility complex (MHC) class II (MHC-II) complexes and co-stimulatory signals from dendritic cells.[7,8] Subsequently, T_{FH} cells upregulate lineage-specific transcription factors such as BCL6, leading to elevated expression of PD-1 and CXCR5.[7,8] After interacting with B cells

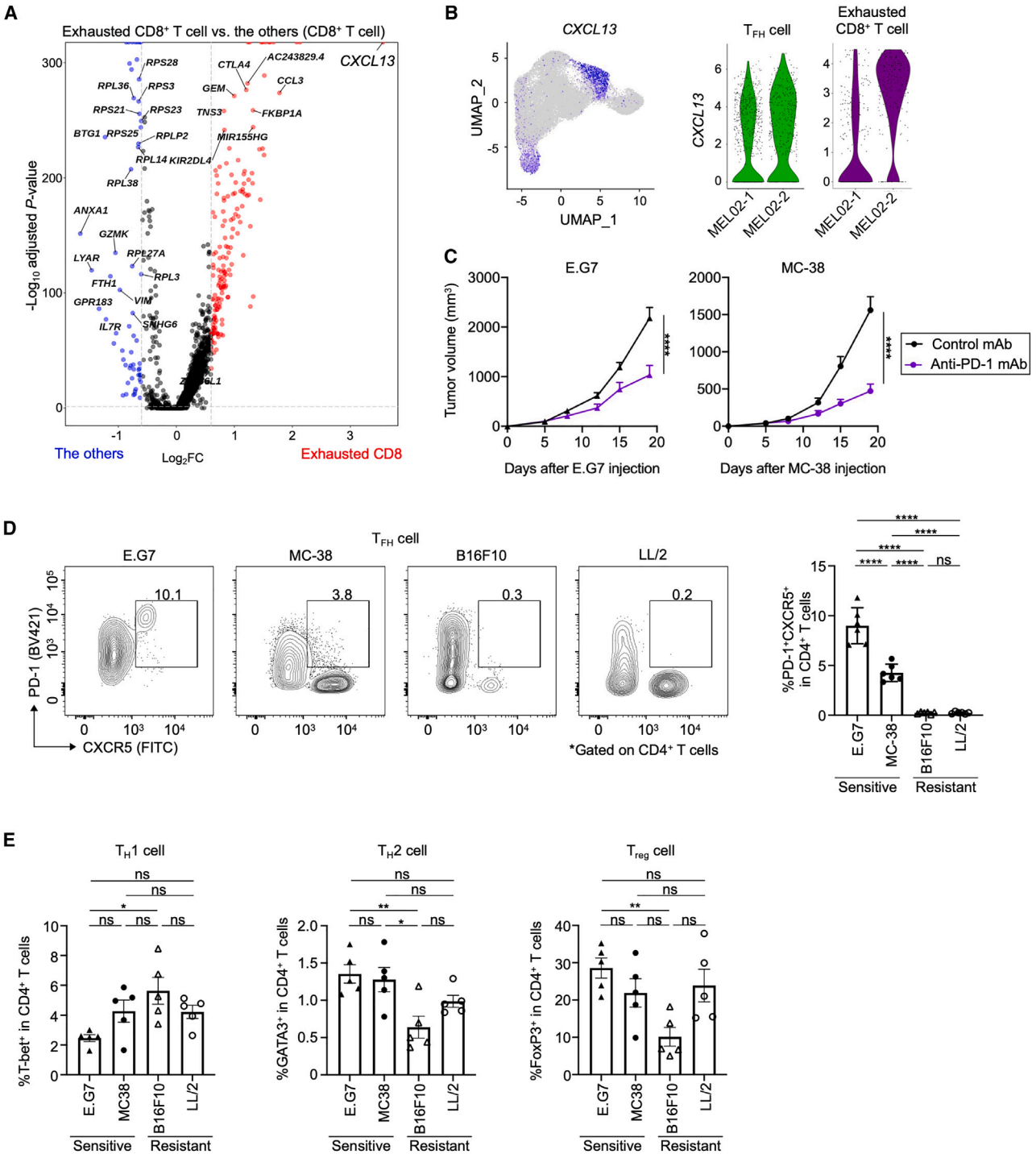

Figure 1. CXCL13 gene expression in scRNA-seq data and T_{FH} cell infiltration in mouse models

(A) Volcano plots in the comparison between exhausted CD8⁺ T cells and other CD8⁺ T cell clusters. Differences in mean expression levels for each gene were compared between exhausted CD8⁺ T cells and the other CD8⁺ T cell clusters. The x axis is plotted as $\log_2$ fold change (FC) for differences in expression levels. The y axis is plotted as p values at $-\log_{10}$. Log_2 FC > 0.6 or < −0.6 and $p < 0.05$ were considered statistically significant. Red dots, significantly upregulated genes in exhausted CD8⁺ T cells; blue dots, significantly downregulated genes in exhausted CD8⁺ T cells.

(B) CXCL13 gene expression. *CXCL13* expression in the uniform manifold approximation and projection (UMAP) figure (left) and the expression change during PD-1 blockade in T_{FH} cell or exhausted CD8⁺ T cell cluster (right) are shown. We used natural logarithm of read counts as the unit.

(legend continued on next page)

at the T-B cell border, T_{FH} cells migrate via CXCR5 response to CXCL13, which is abundant in B cell follicles, to promote germinal center formation, long-lived plasma B cell maturation, and high-affinity antibody production.[7,8] As T_{FH} cells are critical in regulating humoral immunity, the aberrant number and function of T_{FH} cells could cause immunodeficiency and autoimmune diseases.[7,8] Recently, an increasing number of studies have highlighted the role of T_{FH} cells in anti-tumor immunity. In many cancers, intratumoral T_{FH} and B cells and tertiary lymphoid structure (TLS) contribute to anti-tumor immunity and predict longer overall survival and higher response rates to ICIs.[9–18]

We previously reported that PD-1$^+$-exhausted CD8$^+$ T cells in the TME were related to ICI efficacy and that such T cells attacked cancer cells directly (cancer-specific T cells).[19,20] In the present study, we found that such cancer-specific exhausted CD8$^+$ T cells in the TME highly express *CXCL13*, according to single-cell RNA sequencing (scRNA-seq) data for tumor-infiltrating lymphocytes (TILs) of patients with melanoma. In mouse models, CXCL13 produced by tumor-infiltrating PD-1$^+$-exhausted CD8$^+$ T cells recruited T_{FH} cells in the TME, which played important roles in anti-tumor immunity. In addition, the scRNA-seq data for TILs from MHC-II-expressing tumors showed that some tumor-infiltrating T_{FH} cells exhibited cytotoxicity and directly attacked MHC-II-expressing tumors, which was validated in mouse models. The BLIMP1/TCF1 axis determined the differentiation between these non-cytotoxic T_{FH} cells with self-renewal ability and T_{FH}-like cytotoxic CD4$^+$ T cells without self-renewal ability in the TME, which is similar to stem-like progenitor and terminally differentiated exhaustion in CD8$^+$ T cells, respectively.[21,22] We propose a concept of T_{FH}-like CD4$^+$ T cell exhaustion with helper progenitor and cytotoxic differentiated functions, mediating anti-tumor immunity orchestrally with CD8$^+$ T cells.

RESULTS

CXCL13 is highly expressed in tumor-infiltrating cancer-specific exhausted CD8$^+$ T cells

We analyzed tumor-infiltrating T cells from a patient with melanoma (MEL04) who responded to PD-1 blockade therapy with single-cell sequencing (both RNA and T cell receptor [TCR]), as well as three samples, previously published, from two responders (MEL02 and 03) and merged TIL data from these four samples. Patient characteristics are summarized in Table S1. We obtained paired TCR sequences in 17,213 out of 24,724 T cells from four TIL samples (69.3%; Table S2). T cells were classified into nine clusters based on gene expression profiling, as previously reported (Figures S1A–S1C and Table S3).[20,23,24] All samples had a considerable population of exhausted CD8$^+$ T cell cluster, which was characterized by exhaustion-related signature genes such as *PDCD1*, *TNFRSF9*, *ENTPD1*, and *ITGAE* (Figures S1A–S1C), and this cluster showed skewed T cell clones (Figure S1D). Next, we compared gene expression between exhausted CD8$^+$ T cell and the other CD8$^+$ T cell clusters and found that the exhausted CD8$^+$ T cell cluster showed high expression of *CXCL13* (Figures 1A and 1B), which is consistent with the results from previous studies.[17,24–30] Furthermore, exhausted CD8$^+$ T cells were classified into four populations, and *CXCL13* was homogeneously and highly expressed in all populations (Figures S2A and S2B). CXCL13, a ligand for CXCR5, reportedly recruited CXCR5$^+$ T_{FH} cells,[5,6] also exhibiting high *CXCL13* expression (Figure S2C). *CXCL13* expression in exhausted CD8$^+$ T cells and T_{FH} cells in the TME, along with T_{FH} cell infiltration, increased after treatment with anti-PD-1 monoclonal antibody (mAb) in MEL02 (Figures 1B, S1A, and S1E), which is consistent with the results of previous studies.[20,23–25]

Tumor-infiltrating T_{FH} cells play important roles in PD-1 blockade-mediated anti-tumor immunity

We focused on T_{FH} cell infiltration in mouse models, generally defined as PD-1$^+$CXCR5$^+$CD4$^+$ T cells.[5,6] Consistent with this, PD-1$^+$CXCR5$^+$FOXP3$^-$CD4$^+$ T cells gated using isotype controls showed higher Bcl6 expression than non-T_{FH} FOXP3$^-$CD4$^+$ T cells in MC-38 mouse tumors (Figures S3A and S3B). In contrast, T-bet and GATA3 were highly expressed in non-T_{FH} FOXP3$^-$CD4$^+$ T cells (Figures S3A and S3B). We used the E.G7 and MC-38 cell lines as sensitive models to PD-1 blockade and the B16F10 and LL/2 cell lines as resistant models (Figures 1C, and S3C). TIL analyses demonstrated high T_{FH} cell infiltration in the sensitive tumors but low infiltration in the resistant tumors (Figure 1D). However, for T_H1, T_H2, and regulatory T (T_{reg}) cell infiltration, no consistent tendencies were observed between the sensitive and resistant tumors (Figure 1E).

We next evaluated the role of tumor-infiltrating T_{FH} cells in PD-1 blockade-mediated efficacy. As was observed in MEL02, PD-1 blockade increased T_{FH} cell infiltration in the MC-38 sensitive tumor model, consistent with the results from previous scRNA-seq studies (Figures 2A, S1A, and S1E).[20,23–25] We evaluated anti-tumor immunity using T_{FH} cell knockout mice (*Bcl6$^{fl/fl}$Cd4^{cre}* mice) (Figure S3D). While TCF1 expression in CD4$^+$ T cells also decreased in *Bcl6$^{fl/fl}$Cd4^{cre}* mice as previously reported,[31] the frequency of CD44$^+$CD62L$^-$CD4$^+$ effector T cells in TILs and MC-38 tumor growth was comparable with that in control mice (Figures 2B, S3E, and F). Otherwise, PD-1 blockade-mediated efficacy was impaired in *Bcl6$^{fl/fl}$Cd4^{cre}* mice (Figure 2B), similar to the results of previous studies.[17] Accordingly, the activation of CD8$^+$ T cells was also impaired in the T_{FH} cell knockout mice

(C) Efficacy of PD-1 blockade against various tumors. Cells were injected subcutaneously into C57BL/6J mice on day 0, and tumor volume was monitored twice a week. Mice were grouped when the tumor volume reached approximately 100 mm^3, and anti-PD-1 mAb or control mAb was administered intraperitoneally three times every 3 days thereafter.

(D and E) Frequency of the tumor-infiltrating CD4$^+$ T cell population. The cells were injected subcutaneously into C57BL/6J mice on day 0, and the tumors were harvested on day 14 to collect TILs for evaluation. Representative flow cytometry staining of T_{FH} cells (left) and summary of the data (right) are shown in (D). Summaries of other population data (left, T_H1 cells; middle, T_H2 cells; right, T_{reg} cells) are also shown in (E). All *in vivo* experiments were performed in duplicate, and similar results were obtained. Two-way ANOVA was used in (C) and one-way ANOVA with Bonferroni corrections was used in (D) and (E) for statistical analyses. *p < 0.05; **p < 0.01; ****p < 0.0001; ns, not significant; bars, mean; error bars, SEM. See also Figures S1, S2, and S3 and Tables S1, S2, and S3.

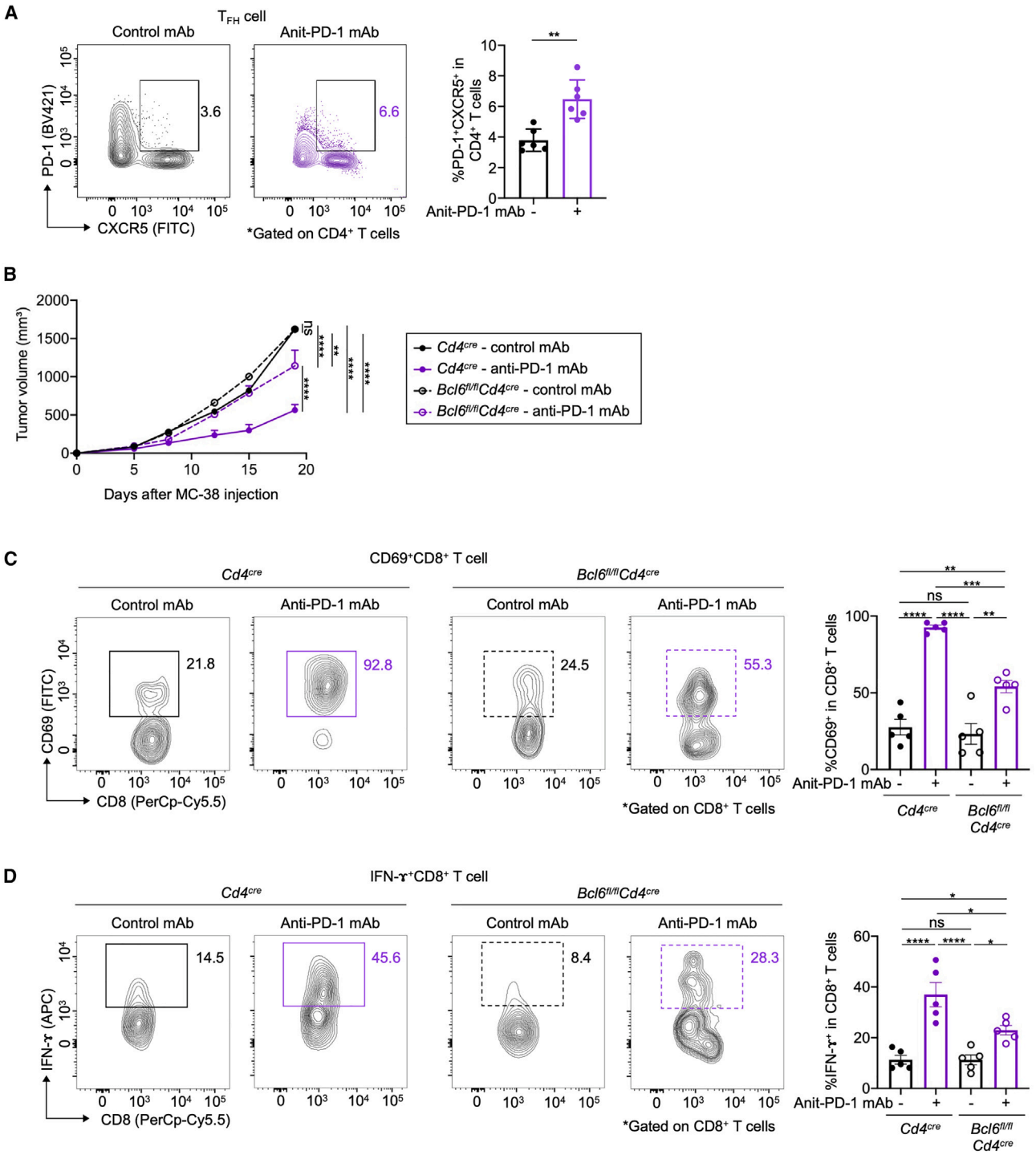

Figure 2. Role of tumor-infiltrating T_{FH} cells in anti-tumor immunity

(A) Frequency of tumor-infiltrating T_{FH} cells subjected to PD-1 blockade. MC-38 cells were injected subcutaneously into C57BL/6J mice on day 0. Mice were grouped when the tumor volume reached approximately 100 mm^3, and anti-PD-1 mAb or control mAb was administered intraperitoneally three times every 3 days thereafter. Tumors were harvested 7 days after treatment initiation to collect TILs for evaluation. Representative flow cytometry staining (left) and summary of these data (right) are shown.

(B) Efficacy of PD-1 blockade in *Cd4*^{cre} or *Bcl6*$^{fl/f}$*Cd4*^{cre} mice. *In vivo* experiments were performed as described in (A) using *Cd4*^{cre} or *Bcl6*$^{fl/fl}$*Cd4*^{cre} mice. Tumor volume was monitored twice a week. The growth curves are shown.

(legend continued on next page)

(Figures 2C and 2D). In addition, high CXCL13 gene expression was related to a good prognosis by PD-1 blockade therapies from a publicly available dataset (Figure S3G).[25] These findings suggest that tumor-infiltrating T_{FH} cells play important roles in PD-1 blockade-mediated anti-tumor immunity.

Tumor-infiltrating exhausted CD8$^+$ T cells recruit T_{FH} cells via CXCL13

Our scRNA-seq data indicated high CXCL13 production in cancer-specific exhausted CD8$^+$ T cells in the TME and prompted us to conduct further *in vitro* and *in vivo* experiments. When antigen clearance fails and exposure is maintained, as observed in chronic infection or cancer, exhaustion may occur in CD8$^+$ T cells.[32,33] Thus, we investigated whether TCR stimulation induces CXCL13 expression. TCR stimulation induced CXCL13 and PD-1 expression, and CXCL13 and PD-1 were co-expressed in CD8$^+$ T cells (Figures 3A–3C). These findings were validated by gene expression (Figure 3D). Accordingly, in the sensitive tumors, CXCL13 was produced by tumor-infiltrating PD-1$^+$CD8$^+$ T cells but not by PD-1$^-$CD8$^+$ T cells from both gene expression and flow cytometric analyses (Figures 3D and 3E). CD8$^+$ T cell deletion by anti-CD8β mAb and CXCL13 blockade by anti-CXCL13 mAb inhibited T_{FH} cell infiltration (Figures 3F and 3G).

Somatic mutation-derived neoantigens, which can be recognized as non-self antigens, reportedly induce strong T cell activation similar to foreign antigens.[34,35] Thus, neoantigens are very important for the ICI response.[35–37] When OVA peptide was introduced into cancer cells as a neoantigen for mice, both CXCL13 production in PD-1$^+$CD8$^+$ T cells and T_{FH} cell infiltration significantly increased (Figures 4A and 4B). Because the full-length OVA peptide reportedly includes both peptide epitopes presented by MHC-I (OVA-I) and MHC-II (OVA-II),[38] we introduced only OVA-I or OVA-II into the cancer cells (Figure S3H), showing that OVA-I, but not OVA-II, increased CXCL13 production by PD-1$^+$CD8$^+$ T cells and T_{FH} cell infiltration (Figures 4A and 4B). Accordingly, *B2m* deletion completely inhibited CXCL13 production and T_{FH} cell infiltration, which was not recovered by MHC-II expression (*mCiita* overexpression) (Figures 4C, 4D, and S3I). These findings indicate that tumor-infiltrating cancer-specific exhausted CD8$^+$ T cells recruit T_{FH} cells via CXCL13 and that TCR stimulation, such as with neoantigens against MHC-I but not MHC-II, promotes CXCL13 production and T_{FH} cell infiltration.

T_{FH} cells exhibit cytotoxicity against MHC-II-expressing tumors

From the scRNA-seq data, we found high *GZMA* expression in a part of the tumor-infiltrating T_{FH} cells (Figures S1A and S1B), as well as two gradient populations in the tumor-infiltrating T_{FH} cells (Figures 5A, S4A. and Table S4). One population was characterized by high expression of cytotoxicity-related genes such as *GZMA/B* and *PRF1* and inflammation-related genes such as *CCL4/5* and *CXCR6* (cytotoxic population) (Figure 5A). Additionally, we analyzed tumor-infiltrating T_{FH} cells extracted from publicly available scRNA-seq data on melanoma, lung cancer, and colorectal cancer TILs.[27,28] As shown in Figure S4B, the T_{FH} cells also had gradient cytotoxic and non-cytotoxic populations in the publicly available scRNA-seq data. Because all melanoma cells used in our study (MEL02-1, MEL02-2, MEL03, and MEL04) showed MHC-II expression, especially after treatment with IFN-γ (Figure 5B), we analyzed the specificities of T_{FH}-like cytotoxic CD4$^+$ T cells from the cytotoxic population against MHC-II-expressing cancer cells. We created several TCR-transduced CD4$^+$ NFAT-Jurkat cell lines from the skewed T_{FH}-like cytotoxic CD4$^+$ T cell clonotype of MEL04 and co-cultured them with MHC-II-expressing MEL04 cells (MEL04/hCIITA) (Figures S5A and S5B; Table S5). Each TCR-transduced NFAT-Jurkat cell line from the cytotoxic population responded to MEL04/hCIITA cells, indicating that these T_{FH}-like cytotoxic CD4$^+$ T cells attacked MHC-II-expressing cancer cells directly (Figure 5C). In addition, we confirmed direct cytotoxicity from killing assays using each TCR-transduced primary CD4$^+$ T cell (Figure 5D). We performed RNA velocity and latent time analysis to identify the polarity of differentiation in non-T_{reg} CD4$^+$ T cells; the results showed that the differentiation of T_{FH} cells, including both populations, from naive CD4$^+$ T cells was different from that of activated or memory CD4$^+$ T cells (Figure S4C). When we focused on T_{FH} cells, the T_{FH}-like cytotoxic CD4$^+$ T cells were at the late stage of differentiation, and some non-cytotoxic T_{FH} cells could differentiate into T_{FH}-like cytotoxic CD4$^+$ T cells (Figures 5E and 5F). We additionally evaluated clonotypes from TCR sequences and found considerable overlapping clonotypes between the gradient cytotoxic and non-cytotoxic populations (Figure 5G). Among the overlapping clonotypes, the cytotoxic population had more expanded clones than the non-cytotoxic population (Figure 5H). These findings suggest that T_{FH}-like cytotoxic CD4$^+$ T cells are differentiated from non-cytotoxic T_{FH} cells. Accordingly, TCRs mainly from the non-cytotoxic population also responded to MEL04/hCIITA cells (Figure 5C), suggesting that both non-cytotoxic T_{FH} cells and T_{FH}-like cytotoxic CD4$^+$ T cells are cancer-specific CD4$^+$ T cells.

We validated these findings using a mouse model. Accordingly, PD-1$^+$CXCR5$^+$CD4$^+$ T_{FH} cells showed cytotoxicity in the TME of MHC-II-expressing tumors, which was increased by PD-1 blockade (Figure 6A). Indeed, T_{FH} cells from *OT-II* mice exhibited cytotoxicity against *OVA*-overexpressing MHC-I$^-$MHC-II$^+$ cancer cells (MC-38/OVA/B2mKO/mCiita) (Figure 6B). Furthermore, T_{FH} cell transfer from *OT-II* mice showed efficacy against *OVA*-overexpressing MHC-I$^-$MHC-II$^+$ tumors but not MHC-II$^-$ tumors *in vivo* (Figures 6C, and S5C). Altogether, a part of the tumor-infiltrating T_{FH} cells directly attacks MHC-II-expressing tumors, and such T_{FH}-like cytotoxic CD4$^+$ T cells are continuously differentiated from non-cytotoxic T_{FH} cells.

(C and D) CD69 expression (C) and IFN-γ production (D) in tumor-infiltrating CD8$^+$ T cells subjected to PD-1 blockade in *Cd4^{cre}* or *Bcl6$^{fl/fl}$Cd4^{cre}* mice. Tumors were harvested 7 days after treatment initiation to collect TILs for evaluation. Representative flow cytometry staining (left) and summary of these data (right) are shown. All *in vivo* experiments were performed in duplicate, and similar results were obtained. One-way ANOVA with Bonferroni corrections was used in (C) and (D), a t test was used in (A), and two-way ANOVA with Bonferroni corrections was used in (B) for statistical analyses. *p < 0.05; **p < 0.01; ***p < 0.001; ****p < 0.0001; ns, not significant; bars, mean; error bars, SEM. See also Figure S3.

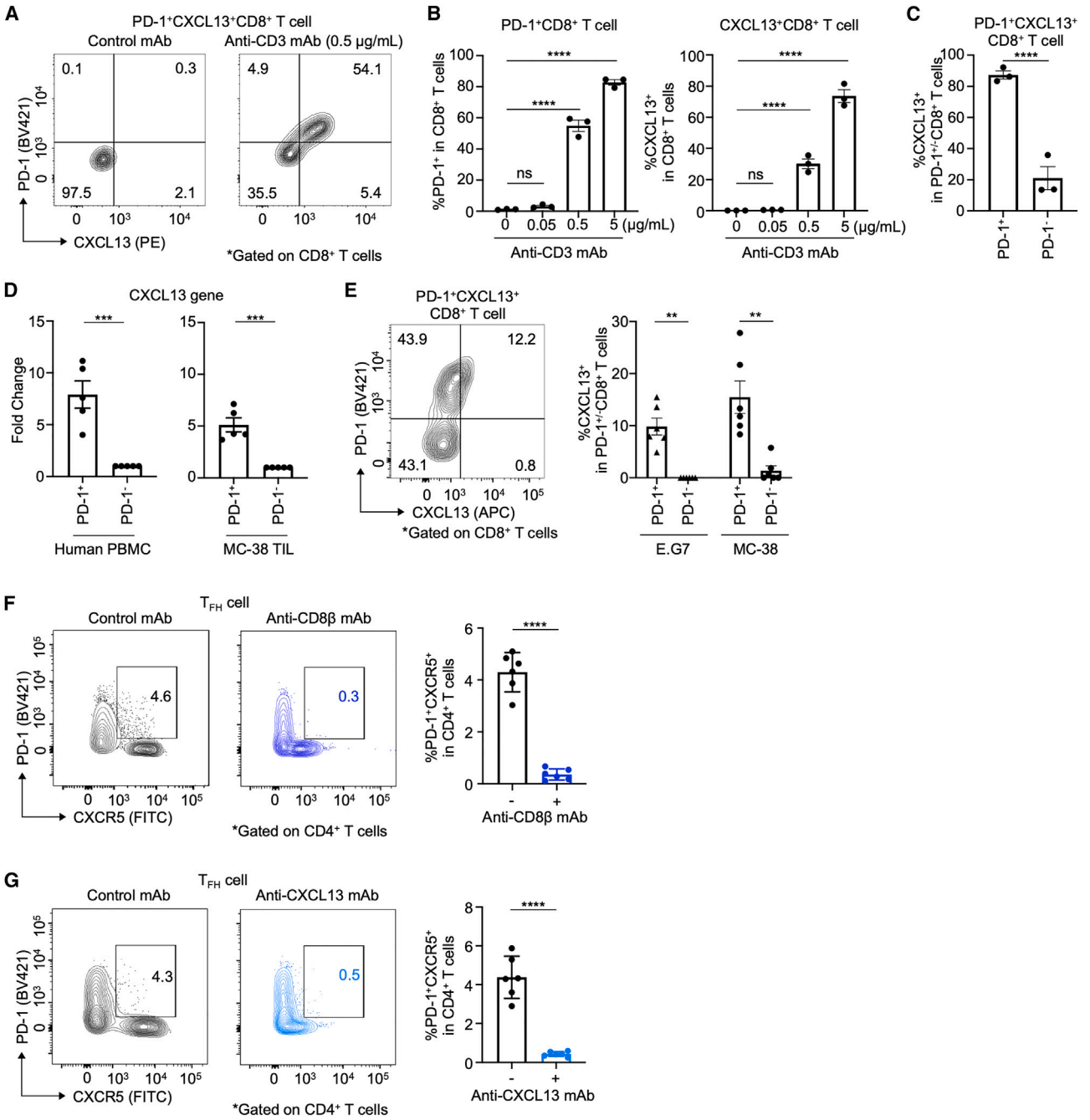

Figure 3. CXCL13 produced by tumor-infiltrating exhausted CD8⁺ T cells and T_{FH} cell infiltration

(A–C) PD-1 and CXCL13 expression in CD8⁺ T cells after TCR stimulation. Peripheral blood mononuclear cells (PBMCs) from healthy donors were stimulated by anti-CD3 and anti-CD28 mAbs for 48 h. PD-1 expression and CXCL13 expression in CD8⁺ T cells were subsequently analyzed with flow cytometry. Representative flow cytometry staining (A) and the expression of PD-1 (B; left) and CXCL13 (B; right) and CXCL13 expression according to PD-1 expression (C) are shown.

(D) CXCL13 gene expression in CD8⁺ T cells. PBMCs from healthy donors were stimulated as described in (A)–(C). Sorted PD-1⁺ or PD-1⁻ CD8⁺ T cells were subsequently analyzed with quantitative reverse transcription PCR. In addition, cancer cells were injected subcutaneously into C57BL/6J mice on day 0, and tumors were harvested on day 14 to collect TILs, from which PD-1⁺ or PD-1⁻ CD8⁺ T cells were sorted and analyzed with quantitative reverse transcription PCR. We calculated FCs to paired PD-1⁻ CD8⁺ T cells and summaries (left, human PBMC; right, MC-38 TIL) are shown.

(E) CXCL13 expression in tumor-infiltrating CD8⁺ T cells in mouse models. *In vivo* experiments were performed as described in (D). Representative flow cytometry staining in the MC-38 tumors and summary of CXCL13 expression according to PD-1 expression are shown.

(legend continued on next page)

The BLIMP1/TCF1 axis determines the differentiation between T_{FH}-like cytotoxic CD4$^+$ T cells and non-cytotoxic T_{FH} cells

We compared gene expression between the gradient cytotoxic and non-cytotoxic populations using scRNA-seq data. The T_{FH}-like cytotoxic CD4$^+$ T cells showed high *PRDM1* and low *TCF7* expression (encoding BLIMP1 and TCF1, respectively) (Figures S4D and S4E). *LAG3* was explicitly expressed in T_{FH}-like cytotoxic CD4$^+$ T cells (Figures S4D and S4E). In publicly available datasets,[27,28] high *PRDM1*/*LAG3* and low *TCF7* expression in T_{FH}-like cytotoxic CD4$^+$ T cells were also observed (Figure S4B). Thus, we analyzed these molecules in TILs of MHC-II-expressing mouse tumors. Consistently, MHC-II$^+$ tumors had more LAG-3$^+$ T_{FH} cell infiltration than MHC-II$^-$ tumors (Figure 7A), and we found high BLIMP1 and low TCF1 expression in LAG-3$^+$ T_{FH} cells and low BLIMP1 and high TCF1 expression in LAG-3$^-$ T_{FH} cells in the TME (Figure 7B). In addition, LAG-3$^+$ T_{FH} cells exhibited greater cytotoxicity in the TME than LAG-3$^-$ T_{FH} cells (Figures 7C, and S6A). Furthermore, the production of cytokines, such as IFN-γ and TNF-α, also increased in LAG-3$^+$ T_{FH} cells in TILs (Figure S6A). In the killing assay, LAG-3$^+$ T_{FH} cells in TILs exhibited greater direct cytotoxicity than LAG-3$^-$ T_{FH} cells (Figure 7D). The cytotoxicity was decreased by *mTcf7* overexpression or *mPrdm1* knockdown in *in vitro* experiments in mouse T_{FH} cells (Figures 7E, and S6B).

According to our scRNA-seq and experimental data, the T_{FH} cell clusters exhibited high *TOX* expression in addition to *PDCD1* expression (Figure S1B), and both non-cytotoxic T_{FH} cells and T_{FH}-like cytotoxic CD4$^+$ T cells are cancer-specific CD4$^+$ T cells, which are similar to exhausted CD8$^+$ T cells.[19,20,40] In addition, non-cytotoxic T_{FH} cells in the TME showed high TCF1 and low BLIMP1/LAG-3 expression; this phenotype is similar to that of stem-like progenitor exhausted CD8$^+$ T cells in the TME.[21,22] In contrast, T_{FH}-like cytotoxic CD4$^+$ T cells showed low TCF1 and high BLIMP1/LAG-3 expression; this phenotype is similar to that of terminally differentiated exhausted CD8$^+$ T cells.[21,22] Stem-like progenitor exhausted CD8$^+$ T cells reportedly maintain the capacity for proliferation, self-renewal ability, and responsiveness to PD-1 blockade, whereas loss of TCF1 with concomitant upregulation of multiple inhibitory immune checkpoint molecules is associated with the terminally differentiated exhaustion phenotype and a further decline in functions.[21,22] Thus, we next analyzed proliferation, apoptosis, and responsiveness to ICIs. Similar to stem-like progenitor exhaustion, LAG-3$^-$ non-cytotoxic T_{FH} cells sorted from TILs were more proliferative, according to 5-(and 6)-carboxyfluorescein diacetate succinimidyl ester (CFSE) staining, and less apoptotic, according to Annexin V staining, than LAG-3$^+$ T_{FH}-like cytotoxic CD4$^+$ T cells (Figures 7F and S6C). Although PD-1 blockade increased cytotoxicity in tumor-infiltrating T_{FH} cells (Figure 6A), these bulk T_{FH} cells included both LAG-3$^-$ and LAG-3$^+$ T_{FH} cells. Thus, we further performed *ex vivo* assays using tumor-infiltrating LAG-3$^-$ and LAG-3$^+$ T_{FH} cells separately. PD-1 single blockade activated not LAG-3$^+$ T_{FH}-like cytotoxic CD4$^+$ T cells but LAG-3$^-$ T_{FH} cells, whereas PD-1 and LAG-3 double blockade activated LAG-3$^+$ T_{FH}-like cytotoxic CD4$^+$ T cells (Figures 7G, and S6D). Overall, both gradient T_{FH}-like CD4$^+$ T cell populations are cancer specific, and the BLIMP1/TCF1 axis determines the differentiation between T_{FH}-like cytotoxic CD4$^+$ T cells with high LAG-3 expression and non-cytotoxic T_{FH} cells with low LAG-3 expression. Particularly, T_{FH}-like cytotoxic CD4$^+$ T cells in the TME directly attack MHC-II-expressing tumors. In addition, non-cytotoxic T_{FH} cells, which are less apoptotic and more proliferative, respond to PD-1 single blockade, whereas T_{FH}-like cytotoxic CD4$^+$ T cells, which are more apoptotic and less proliferative, do not respond. These gradient T_{FH}-like CD4$^+$ T cell populations are similar to stem-like progenitor and terminally differentiated exhausted CD8$^+$ T cells (Figure S6E).

A previous study using a chronic infection model classified CD4$^+$ T cells into naive CD4$^+$ T cell, progenitor CD4$^+$ T cell, effector CD4$^+$ T cell, T_{FH} cell, and T_{reg} cell clusters.[31] To align with this previous study, we extracted non-naive/non-T_{reg} cells from the CD4$^+$ T cells and reclassified them into progenitor CD4$^+$ T cell, effector CD4$^+$ T cell, and T_{FH} cell clusters (including non-cytotoxic and cytotoxic populations) (Figure S4F). *PDCD1*, *CXCR5*, *ICOS*, *CD200*, and *CXCL13* were highly expressed in T_{FH} cell clusters compared to the progenitor or effector CD4$^+$ T cell clusters. High *CCR7* and *CD69* expression was observed in the progenitor and effector CD4$^+$ T cells, respectively. *TCF7* expression in the non-cytotoxic T_{FH} cells was as high as that in the progenitor CD4$^+$ T cells, suggesting that the non-cytotoxic T_{FH} cells had progenitor-like functions. Cytotoxicity was the strongest in T_{FH}-like cytotoxic CD4$^+$ T cells, along with high *LAG3*/*PRDM1* and low *TCF7* expression. In addition, considerably overlapping TCR clonotypes between the cytotoxic and non-cytotoxic T_{FH} cell populations were observed, whereas there were few overlapping between the progenitor or effector CD4$^+$ T cell cluster and T_{FH} cell clusters (Figure S4G), suggesting a different differentiation between the identified gradient T_{FH} cell populations and previously reported progenitor or effector clusters.

T_{FH}-like cytotoxic CD4$^+$ T cells increase in the TME after PD-1 blockade

We analyzed the kinetic changes in these T_{FH} cell clusters in the TME of MHC-II-expressing tumors during PD-1 blockade at several time points (day 5, immediately before PD-1 blockade; days 14 and 21). As shown in Figure S7A, the frequency of total T_{FH} cells increased in the TME over time, even in the absence of PD-1 blockade. Additionally, PD-1 blockade further increased this cluster. TCR repertoire analyses revealed that novel TCRs

(F and G) Frequency of tumor-infiltrating T_{FH} cells treated with anti-CD8β mAb (F) or anti-CXCL13 mAb (G). *In vivo* experiments were performed as described in (D). Anti-CD8β mAb or control mAb was administered intraperitoneally on days −1 and 6. Anti-CXCL13 mAb or control mAb was administered intraperitoneally three times in a week. Tumors were harvested on day 14 to collect TILs for evaluation. Representative flow cytometry staining (left) and summary of these data (right) are shown. All *in vitro* experiments were performed in triplicate, and all *in vivo* experiments were performed in duplicate, and similar results were obtained. One-way ANOVA with Bonferroni corrections was used in (B), and t tests were used in (C)–(G) for statistical analyses. **p < 0.01; ***p < 0.001; ****p < 0.0001; ns, not significant; bars, mean; error bars, SEM. See also Figure S3.

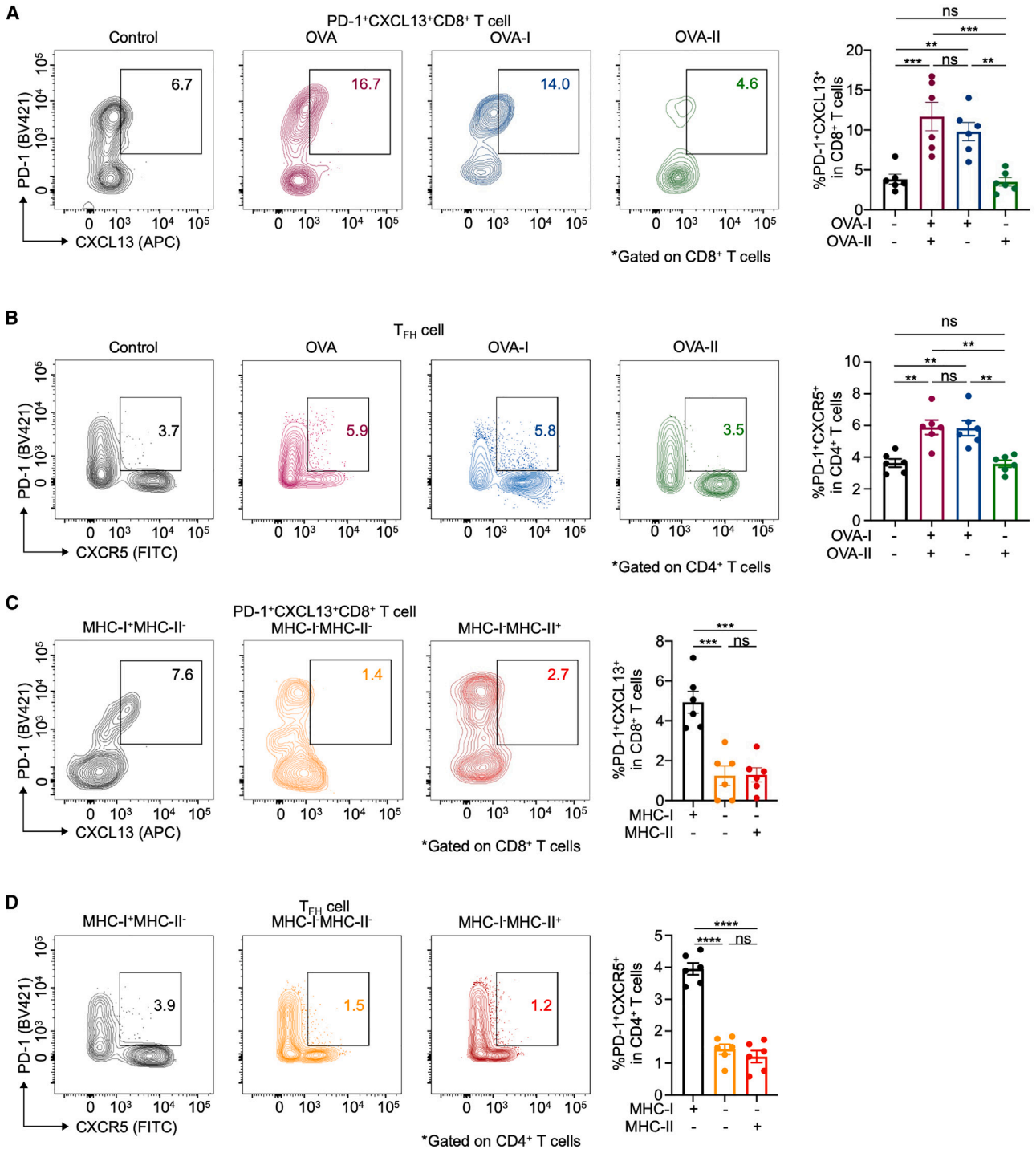

Figure 4. Antigenicity of MHC-I, CXCL13 production, and T_{FH} cell infiltration

(A and B) Frequencies of tumor-infiltrating PD-1$^+$CXCL13$^+$CD8$^+$ T cells (A) and T_{FH} cells (B) according to antigenicity. MC-38 (control), MC-38/OVA, MC-38/OVA-I, or MC-38/OVA-II cells were injected subcutaneously into C57BL/6J mice on day 0, and tumors were harvested on day 14 to collect TILs for evaluation. Representative flow cytometry staining (left) and summary of these data (right) are shown.

(C and D) Frequencies of tumor-infiltrating PD-1$^+$CXCL13$^+$CD8$^+$ T cells (C) and T_{FH} cells (D) according to MHC expression. *In vivo* experiments were performed as described in (A) and (B) using MC-38 (MHC-I$^+$MHC-II$^-$), MC-38/B2mKO (MHC-I$^-$MHC-II$^-$), or MC-38/B2mKO/mCiita (MHC-I$^-$MHC-II$^+$) cells. Representative flow cytometry staining (left) and summary of these data (right) are shown. All *in vivo* experiments were performed in duplicate, and similar results were obtained. One-way ANOVA with Bonferroni corrections was used in (A)–(D) for statistical analyses. **p < 0.01; ***p < 0.001; ****p < 0.0001; ns, not significant; bars, mean; error bars, SEM. See also Figure S3.

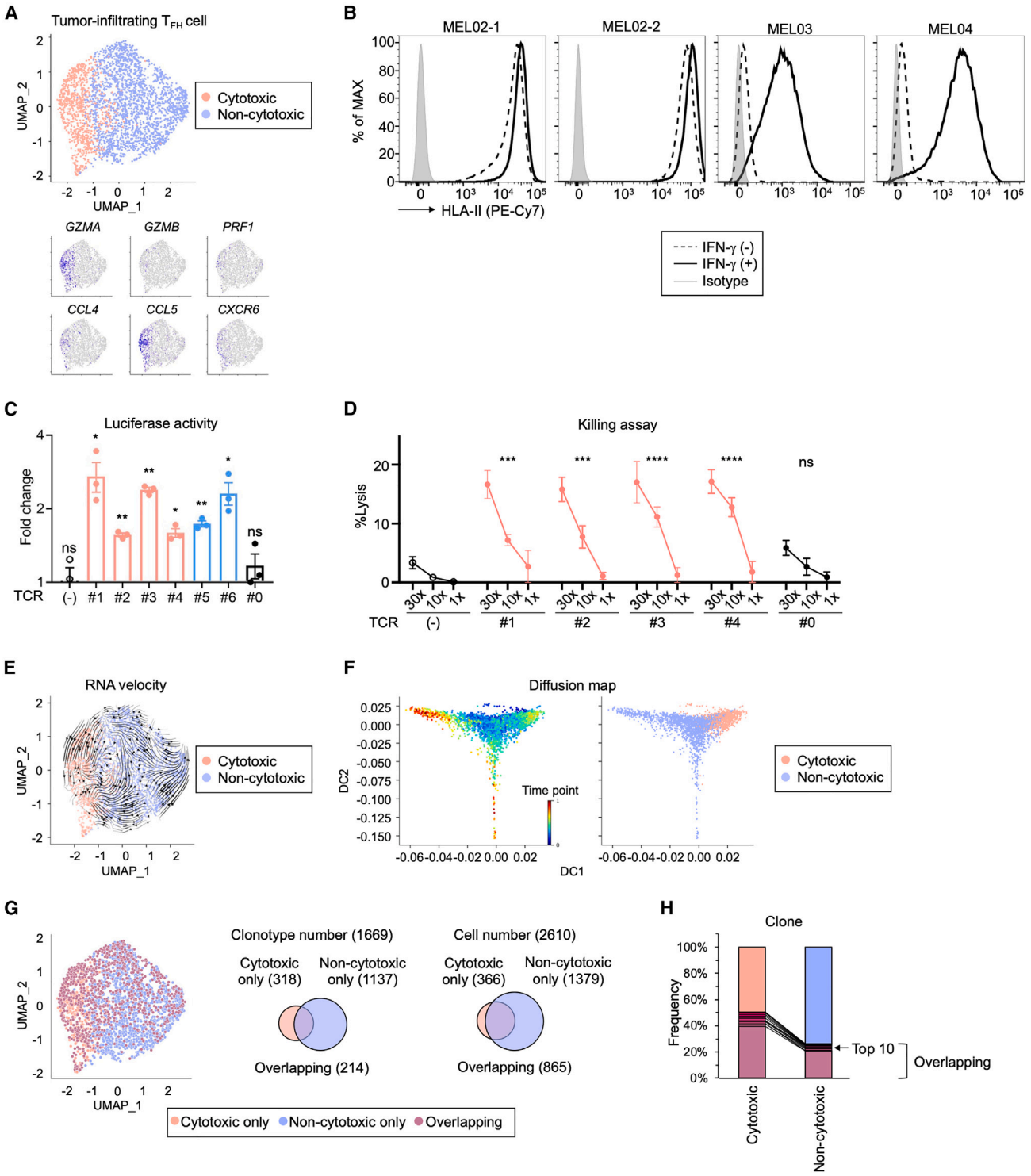

Figure 5. Further classification of tumor-infiltrating T_{FH} cells into cytotoxic and non-cytotoxic populations

(A) Populations in tumor-infiltrating T_{FH} cells. Tumor-infiltrating T_{FH} cells were extracted from the merged data of four samples, which were reclassified into two populations. UMAP figure (top) and representative cytotoxicity-related or inflammation-related genes (bottom) are shown.

(B) MHC-II expression in melanoma cell lines. Cancer cells were treated with or without IFN-γ for 24 h and subsequently analyzed with flow cytometry. Representative flow cytometry staining is shown.

(C) Reactivity of each T cell clonotype from the cytotoxic or non-cytotoxic population. Each TCR from the cytotoxic or non-cytotoxic population of MEL04 was transduced into $CD4^+$ NFAT-Jurkat cells. All TCR-transduced $CD4^+$ NFAT-Jurkat cells were co-cultured with MHC-II-expressing MEL04/hCIITA cells. 24 hours

(legend continued on next page)

were increased in tumor-infiltrating T_{FH} cells after PD-1 blockade (Figure S7B). However, the frequency of GZMB$^+$ cytotoxic T_{FH} cells temporarily increased in the TME but decreased without PD-1 blockade (Figure S7C). PD-1 blockade increased infiltration, but this tendency was similar to that observed without PD-1 blockade (Figure S7C). Similarly, PD-1 blockade increased cytotoxic T_{FH} cell infiltration in the TME of MEL02 (Figure S7D). Clonal replacement of tumor-infiltrating T_{FH} cells was observed in MEL02 (Figure S7E), similar to exhausted CD8$^+$ T cells in the TME, as we previously reported.[20] Particularly, most cytotoxic T_{FH} cell clonotypes in the TME before PD-1 blockade (MEL02-1) disappeared after treatment (MEL02-2), but some non-cytotoxic T_{FH} cell clonotypes remained cytotoxic T_{FH} cells after the treatment (Figure S7E). This indicates that increased cytotoxic T_{FH} cell clonotypes mainly originate from outside the TME; however, some of them are differentiated from non-cytotoxic T_{FH} cell clonotypes, which is consistent with stem-like progenitor and terminally differentiated exhaustion features in non-cytotoxic and cytotoxic T_{FH} cells, respectively. We also analyzed other CD4$^+$ T cell populations in the TME. Although each population was small, we found that the kinetic changes in the total T_H1 and GZMB$^+$ T_H1 cell infiltration were similar to those in the total T_{FH} and GZMB$^+$ cytotoxic T_{FH} cell infiltration without PD-1 blockade, respectively (Figures S7F and S7G). PD-1 blockade further increased infiltration, but the tendency was similar to that observed without PD-1 blockade (Figure S7F).

DISCUSSION

High PD-1 expression, a feature of T_{FH} cells,[7,8] suggests that PD-1 blockade therapies can produce effects on T_{FH} cells in the TME. Consistent with our study, previous studies with human clinical samples have shown that PD-1 blockade increases tumor-infiltrating T_{FH} cells.[20,23–25] In addition, several previous studies have demonstrated that CXCL13 produced by tumor-infiltrating exhausted CD8$^+$ T cells contributes to T_{FH} cell infiltration and that tumor-infiltrating T_{FH} cells play important roles in anti-tumor immunity.[9–18,24–30] In particular, T_{FH} cell mediated interleukin (IL)-21, B cell maturation, and TLS formation reportedly play important roles in anti-tumor immunity, including PD-1 blockade-mediated immunity.[9–18,41] While these previous studies mainly focused on such helper functions,[9–18,41] we validated the cancer specificity of T_{FH} cells and identified T_{FH}-like cytotoxic CD4$^+$ T cells that attack MHC-II-expressing tumors directly. Furthermore, the same clonotypes were considerably found in both cytotoxic and non-cytotoxic populations, suggesting that a continuous differentiation can be observed between both gradient populations and that such cancer-specific CD4$^+$ T cell clonotypes contribute to anti-tumor immunity via both helper and cytotoxic functions. While recent studies have shown the cytotoxic effect of similar T_{FH}-like CD4$^+$ T cells,[42–44] we have additionally demonstrated that non-cytotoxic T_{FH} cells exhibit a stem-like progenitor exhaustion phenotype with high TCF1 and low BLIMP1/LAG-3 expression and that T_{FH}-like cytotoxic CD4$^+$ T cells exhibit a terminally differentiated exhaustion phenotype with low TCF1 and high BLIMP1/LAG-3 expression. PD-1 single blockade could activate non-cytotoxic T_{FH} cells but not T_{FH}-like cytotoxic CD4$^+$ T cells, whereas PD-1/LAG-3 double blockade could activate T_{FH}-like cytotoxic CD4$^+$ T cells. Similar findings have been reported for CD8$^+$ T cell exhaustion.[21,22] Thus, these findings provide deep insights into cancer-specific T_{FH}-like CD4$^+$ T cell exhaustion with both helper progenitor and cytotoxic differentiated functions, resembling CD8$^+$ T cell exhaustion. Overall, tumor-infiltrating cancer-specific exhausted CD8$^+$ T cells recruit cancer-specific T_{FH}-like CD4$^+$ T cells in the TME via CXCL13, orchestrally mediating anti-tumor immunity via both helper and cytotoxic functions.

We have demonstrated that tumor-infiltrating exhausted CD8$^+$ T cells that directly attack cancer cells recruit T_{FH} cells via CXCL13, consistent with previous reports.[17,24–30] Furthermore, CXCL13 reportedly contributes to B cell recruitment and TLS formation, which is related to a good prognosis and good response to immunotherapies.[9–18,41] Previous studies showed that TGF-β with TCR stimulation induced CXCL13 expression in CD8$^+$ T cells[17] and that TGF-β mediated T_{FH} cell differentiation.[45] In addition to these findings, we determined that strong TCR stimulation is important for CXCL13 production by tumor-infiltrating exhausted CD8$^+$ T cells, both *in vitro* and *in vivo*, particularly using *OVA*-overexpressing tumors. Thus, the neoantigen presented by MHC-I, which can induce strong TCR stimulation, could promote T_{FH} cell infiltration via CXCL13. However, MHC-II

after co-culture, luciferase activity was analyzed. We compared the data with those from experiments without MEL04/hCIITA cells for statistical analyses and calculated the FC. The control clonotype TCR #0 was selected from a minor CD4$^+$ T cell clone in the TME that were frequently found in MHC-matched Adaptive Biotechnologies public peripheral blood datasets.[39]

(D) Killing assay. Calcein-AM-labeled MEL04/hCIITA cells (target cells; T) were co-cultured with each TCR-transduced CD4$^+$ T cell (effector cells; E) at the indicated E/T ratios and subsequently centrifuged. Three hours later, fluorescence was measured.

(E) RNA velocity in T_{FH} cells. We used the velocyto and scVelo software for RNA velocity analysis to predict the direction of cell differentiation in T_{FH} cells. The RNA velocity (direction and speed of migration) of individual cells was estimated from the ratio of unspliced/spliced in the mRNA count data for each gene. The obtained RNA velocities are projected as arrows in the UMAP figure. Long arrows represent rapid differentiation.

(F) Latent time in T_{FH} cells. The latent time represents the real time experienced by cells as they differentiate; it was calculated from RNA velocity. We applied diffusion maps as a nonlinear dimensionality reduction technique to determine the direction of cell differentiation. Latent time (left) and cell type (right) are shown in the diffusion maps.

(G and H) Clonotype classification of tumor-infiltrating T_{FH} cells (G) and the expansion of overlapping clonotypes (H). When all cells were classified into the cytotoxic or the non-cytotoxic population, such clonotypes were named as cytotoxic only or non-cytotoxic only clonotypes, respectively. The others were named as overlapping clonotypes. Plots of three categorized clonotypes in the UMAP figure (G; left) and Venn diagram of clonotype number (G; middle) or cell number (G; right) are shown. Expansion of overlapping clonotypes is shown in (H). An arrow indicates top 10 overlapping clonotypes. *In vitro* experiments were performed in triplicate; t tests were used in (C) for statistical analyses. In (D), the area under the curve values for the killing curve was calculated, and one-way ANOVA with Bonferroni corrections was used for comparing the area under the curve values. *$p < 0.05$; **$p < 0.01$; ***$p < 0.001$; ****$p < 0.0001$; ns, not significant; bars, mean; error bars, SEM. See also Figures S4 and S5, and Tables S1, S2, S4, and S5.

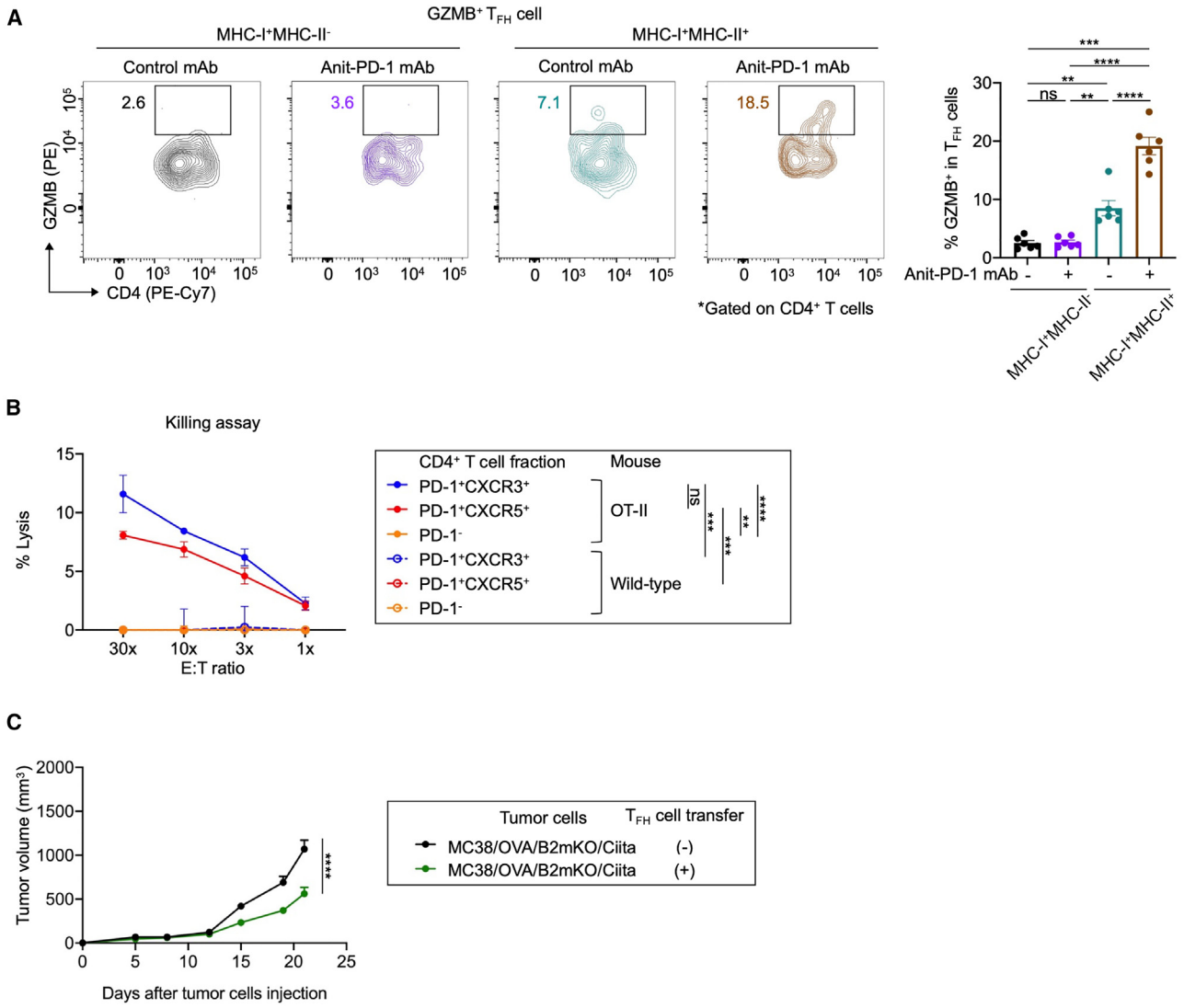

Figure 6. Cytotoxicity of T_{FH} cells against MHC-II-expressing mouse tumors

(A) GZMB expression in T_{FH} cells according to MHC expression. MC-38 (MHC-I$^+$MHC-II$^-$) or MC-38/mCiita (MHC-I$^+$MHC-II$^+$) cells were injected subcutaneously into C57BL/6J mice. Mice were grouped when the tumor volume reached approximately 100 mm^3, and anti-PD-1 mAb or control mAb was administered intraperitoneally three times every 3 days thereafter. Tumors were harvested 7 days after the initiation of treatment to collect TILs for evaluation. Representative flow cytometry staining (left) and summary of these data (right) are shown.

(B) Killing assay for T_{FH} cells. PD-1$^+$CXCR3$^+$, PD-1$^+$CXCR5$^+$, or PD-1$^-$ CD25$^-$CD4$^+$ T cells were sorted from *OT-II* or C57BL/6J (wild-type) splenocytes. Calcein-AM-labeled MC-38/OVA/B2mKO/mCiita cells (MHC-I$^-$MHC-II$^+$) (target cells; T) were co-cultured with each T cell (effector cells; E) at the indicated E/T ratios and subsequently centrifuged. 3 hours later, fluorescence was measured.

(C) Efficacy of T_{FH} cell adaptive transfer. MC-38/OVA/B2mKO/mCiita cells (MHC-I$^-$MHC-II$^+$) were injected subcutaneously into B6 SCID mice on day 0. Mice were injected intraperitoneally with or without 2 × 10^6 T_{FH} cells sorted from *OT-II* splenocytes on days 0, 4, and 10. Tumor volume was monitored twice a week. All *in vitro* experiments were performed in triplicate, and all *in vivo* experiments were performed in duplicate, and similar results were obtained. One-way ANOVA with Bonferroni corrections was used in (A), and two-way ANOVA was used in (C) for statistical analyses. In (B), the area under the curve values for the killing curve were calculated, and one-way ANOVA with Bonferroni corrections was used for comparing the area under the curve values. **p < 0.01; ***p < 0.001; ****p < 0.0001; ns, not significant; bars, mean; error bars, SEM.

expression in cancer cells was not related to T_{FH} cell infiltration. Consistent with this result, several studies have shown high *CXCL13* expression in neoantigen-reactive CD8$^+$ T cells in the TME.[27,28] Thus, tumor-infiltrating exhausted CD8$^+$ T cells recognize neoantigens and directly attack cancer cells, producing CXCL13, recruiting T_{FH} and B cells in the TME, and promoting TLS formation. These results indicate that exhausted CD8$^+$ T cells and T_{FH} cells in the TME synergistically contribute to anti-tumor immunity.

Cytotoxic CD4$^+$ T cells are found in mice and humans in various pathological conditions, including cancer.[46–50] Several attempts have been made to define markers, including

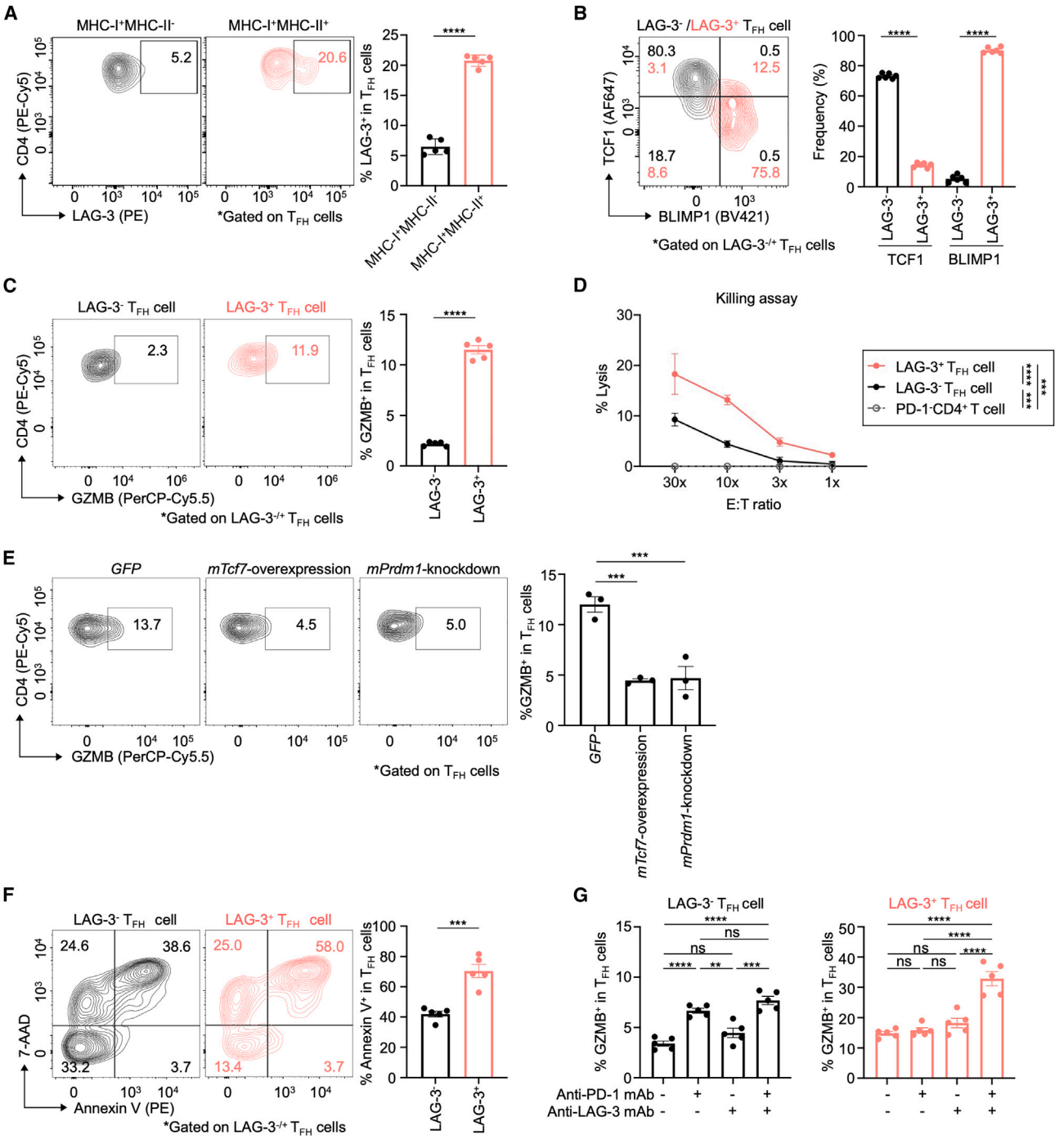

Figure 7. Stem-like progenitor and terminally differentiated exhaustion phenotypes of T_{FH}-like CD4$^+$ T cells in the TME

(A) LAG-3 expression according to MHC-II expression. MC-38 (MHC-I$^+$MHC-II$^-$) or MC-38/mCiita (MHC-I$^+$MHC-II$^+$) cells were injected subcutaneously into C57BL/6J mice. Tumors were harvested on day 14 to collect TILs for evaluation. Representative flow cytometry staining (left) and summary of these data (right) are shown.

(B) TCF1 and BLIMP1 expression in tumor-infiltrating T_{FH} cells according to LAG-3 expression. MC-38/mCiita (MHC-I$^+$MHC-II$^+$) cells were injected subcutaneously into C57BL/6J mice. Tumors were harvested on day 14 to collect TILs for evaluation. Representative flow cytometry staining (left) and summary of these data (right) are shown.

(C) GZMB expression in tumor-infiltrating T_{FH} cells according to LAG-3 expression. *In vivo* experiments were performed as described in (B). TILs were treated with anti-CD3 and CD28 mAbs 6 h before flow cytometry analyses. Representative flow cytometry staining (left) and summary of these data (right) are shown.

(legend continued on next page)

transcription factors that characterize cytotoxic $CD4^+$ T cells; however, no consensus has been reached regarding the existence of such markers. Granzyme or perforin-secreting cytotoxic $CD4^+$ T cells exhibit activation markers, cytokines, and transcription factors associated with different T_H cell subsets.[51,52] T-bet and Eomes are potential candidates for transcription factors because of their well-established role in controlling T_H1 cell responses and inducing granzyme and perforin expression in $CD8^+$ T and natural killer cells.[53] A study in a virus infection model showed that the cytotoxic program does not correlate with T-Bet or Eomes expression and instead is in direct opposition to the Bcl-6-driven T_{FH} cell differentiation program.[54] These virus-induced cytotoxic T cells exhibit higher expression of BLIMP1, which was previously shown to inhibit Bcl-6 and TCF1 expression in $CD4^+$ T cells.[55–57] Similarly, we identified T_{FH}-like cytotoxic $CD4^+$ T cells that directly attack cancer cells in the TME and are regulated by the BLIMP1/TCF1 axis. Additionally, a previous transcriptional analysis of the acquisition of the cytotoxic program in $CD4^+$ T cells revealed that the development of cytotoxic $CD4^+$ T cells in the TME depended on BLIMP1 but not on the T_H1 cell transcriptional program factors (T-bet and Eomes).[48] Furthermore, recent studies demonstrated that neoantigen-specific $CD4^+$ T cells had cytotoxic activity with T_{FH} cell-like phenotype[27,28,42] and that PD-1 and ICOS coexpression, similar to the T_{FH} cell phenotype, reportedly marks tumor-reactive $CD4^+$ T cells.[58] While these findings are consistent with our present study showing the cancer specificity of T_{FH}-like $CD4^+$ cells, we demonstrated the strong direct cytotoxicity of T_{FH}-like cytotoxic $CD4^+$ T cells and the weak cytotoxicity of non-cytotoxic T_{FH} cells against MHC-II-expressing cancer cells. In addition, we observed overlapping clonotypes and continuous differentiation between T_{FH}-like cytotoxic $CD4^+$ T cells and non-cytotoxic T_{FH} cells. Our trajectory analyses have also shown that the differentiation of T_{FH}-like $CD4^+$ T cells, including both populations, from naive $CD4^+$ T cells is different from that of other $CD4^+$ T cells and that the T_{FH}-like cytotoxic $CD4^+$ T cells are at the late stage of differentiation from non-cytotoxic T_{FH} cells. Similar T_{FH}-like cytotoxic $CD4^+$ T cells have been identified in the available scRNA-seq datasets for TILs from melanoma, lung cancer, and colorectal cancer.[27,28] Altogether, TCF1, which inhibits BLIMP1, maintains the differentiation of cancer-specific non-cytotoxic T_{FH} cells with helper function, and BLMP1, which inhibits TCF1, promotes the differentiation of cancer-specific T_{FH}-like cytotoxic $CD4^+$ T cells in the TME from the same clonotypes; both mediate anti-tumor immunity.

TCF1 reportedly plays a crucial role in stem-like progenitor-exhausted $CD8^+$ T cells, which maintain the capacity for proliferation and responsiveness to PD-1 blockade.[21,22] In contrast, loss of TCF1 with concomitant upregulation of multiple inhibitory immune checkpoint molecules is associated with the terminally differentiated exhaustion phenotype and a further decline in function.[21,22] A recent study has shown that Bcl-6-dependent $TCF1^+$ progenitor cells maintain effector and helper $CD4^+$ T cell responses to persistent antigen.[31] In our present study, non-cytotoxic T_{FH} cells with high TCF1 and low BLIMP1/LAG-3 expression were more proliferative and less apoptotic with responsiveness to PD-1 blockade than T_{FH}-like cytotoxic $CD4^+$ T cells with low TCF1 and high BLIMP1/LAG-3 expression, which were less proliferative and more apoptotic without responsiveness to PD-1 blockade. Accordingly, detailed clonotype analyses revealed that most cytotoxic T_{FH} cell clonotypes in the TME before PD-1 blockade disappeared after treatment; however, some of the non-cytotoxic T_{FH} cell clonotypes remained T_{FH}-like cytotoxic $CD4^+$ T cells after the treatment. This relationship between non-cytotoxic T_{FH} cells and T_{FH}-like cytotoxic $CD4^+$ T cells appears to be similar to that between stem-like progenitor and terminally differentiated exhaustion in $CD8^+$ T cells.[21,22] We previously reported high PD-1 and LAG-3 expression in tumor-infiltrating $CD4^+$ T cells in MHC-II-expressing tumors in mouse models.[49] They appear to serve as good markers for T_{FH}-like cytotoxic $CD4^+$ T cells in the TME, and they are so-called exhaustion-related molecules,[59] suggesting that our identified $CD4^+$ T cells could be called exhausted $CD4^+$ T cells.[60,61] In particular, the T_{FH} cell cluster showed high *TOX* expression, which is noted in $CD8^+$ T cell exhaustion, as TOX has recently been found to initiate the epigenetic changes associated with the exhausted phenotype.[40] Considering their features, cancer-specific non-cytotoxic T_{FH} cells and T_{FH}-like cytotoxic $CD4^+$ T cells with continuous differentiation with respect to each other could correspond to stem-like progenitor and terminally differentiated exhausted $CD4^+$ T cells, respectively, resembling cancer-specific exhausted $CD8^+$ T cells.

While similar T_{FH} cell populations have been reported mainly in viral infection settings,[43,54] we also identified them in the TME.

(D) Killing assay. MC-38/mCiita ($MHC\text{-}I^+MHC\text{-}II^+$) cells were injected subcutaneously into OT-II mice. Tumors were harvested on day 14 to collect TILs. $LAG\text{-}3^+$ T_{FH}, $LAG\text{-}3^-$ T_{FH}, or $PD\text{-}1^-$ $CD4^+$ T cells were sorted from the TILs, which were subsequently used for killing assays. Calcein-AM-labeled MC-38/OVA/B2mKO/mCiita cells ($MHC\text{-}I^-MHC\text{-}II^+$) (target cells; T) were co-cultured with each T cell (effector cells; E) at the indicated E/T ratios and subsequently centrifuged. Three hours later, fluorescence was measured.

(E) GZMB expression in *mTcf7*-overexpressing or *mPrdm1*-knockdown T_{FH} cells. Splenocytes from C57BL/6J mice were expanded, into which each lentiviral vector was transduced 4 days after expansion, resulting in *mTcf7* overexpression or *mPrdm1* knockdown. These cells were stimulated with anti-CD3 and CD28 mAbs for 6 h and analyzed with flow cytometry. Representative flow cytometry staining (left) and summary of these data (right) are shown.

(F) Apoptosis in tumor-infiltrating T_{FH} cells according to LAG-3 expression. Apoptosis of sorted $LAG\text{-}3^-$ or $LAG\text{-}3^+$ T_{FH} cells from MC-38/mCiita tumors 14 days after inoculation was evaluated by flow cytometry using Annexin V 3 days after the treatment with anti-CD3 and CD28 mAbs. Representative flow cytometry staining (left) and summary of these data (right) are shown.

(G) GZMB expression in tumor-infiltrating T_{FH} cells subjected to PD-1 and/or LAG-3 blockade. *Ex vivo* experiments were performed as described in (F). Anti-PD-1 mAb and/or anti-LAG-3 mAb were added at the same time with stimulation. Twenty-four hours later, cells were analyzed using flow cytometry. Summaries of these data are shown. All *in vitro* experiments were performed in triplicate, and all *in vivo* and *ex vivo* experiments were performed in duplicates with similar results; t tests were used in (A)–(C) and (F), and one-way ANOVA with Bonferroni corrections was used in (E) and (G) for statistical analyses. The area under the curve values for the killing curve were calculated, and a one-way ANOVA with Bonferroni correction was used to compare the area under the curve values in (D). $^{**}p < 0.01$; $^{***}p < 0.001$; $^{****}p < 0.0001$; ns, not significant; bars, mean; error bars, SEM. See also Figures S6 and S7.

Furthermore, in addition to the clonal linkage of two gradient T_{FH} cell populations in TILs, we found different features, especially TCF1 high/BLIMP1 low stem-like and TCF1 low/BLIMP1 high terminally differentiated features, and demonstrated direct cytotoxicity and differentiation determined by the TCF1/BLIMP1 axis. In a recent study using a chronic infection model, non-naive/non-T_{reg} $CD4^+$ T cells were classified into progenitor, effector, and T_{FH} cell clusters.[31] According to these data, we classified the non-naive/non-T_{reg} $CD4^+$ T cells into three clusters, including the gradient T_{FH} cell populations. Based on gene expression and overlapping TCRs, our identified T_{FH} cell populations seemed to be different from previously reported progenitor or effector $CD4^+$ T cell clusters; however, non-cytotoxic T_{FH} cells had progenitor-like functions. Accordingly, our trajectory analyses have also shown that the differentiation of T_{FH} cells, including both populations, from naive $CD4^+$ T cells differs from that of other $CD4^+$ T cells.

Another previous study of a virus infection revealed that PD-1 and LAG-3 blockade promoted cytotoxic $CD4^+$ T cell differentiation rather than T_{FH} cell differentiation,[54] and we previously reported high PD-1 and LAG-3 expression in tumor-infiltrating $CD4^+$ T cells in MHC-II-expressing tumors in mouse models.[49] Additionally, our present study has demonstrated that not PD-1 single blockade but PD-1 and LAG-3 double blockade reactivates T_{FH}-like cytotoxic $CD4^+$ T cells. Therefore, PD-1 and LAG-3 are promising therapeutic targets for T_{FH}-like cytotoxic $CD4^+$ T cells. Indeed, melanoma reportedly has high frequencies of MHC-II expression in cancer cells, as observed in our present study,[62] and LAG-3 blockade combined with PD-1 blockade exhibited efficacy against advanced melanoma in a recent phase III trial.[63]

In summary, we have demonstrated the importance of tumor-infiltrating exhausted $CD8^+$ T cells and antigen stimulation via MHC-I (i.e., neoantigens) in recruiting T_{FH} cells via CXCL13, which contributes to anti-tumor immunity. In addition, we identified T_{FH}-like cytotoxic $CD4^+$ T cells that directly attack MHC-II-expressing cancer cells in the TME. The same clonotypes and continuous differentiation were observed between T_{FH}-like cytotoxic $CD4^+$ T cells and non-cytotoxic T_{FH} cells, indicating that both populations are cancer-specific $CD4^+$ T cells. In addition, the BLIMP1/TCF1 axis regulated the development of these cytotoxic $CD4^+$ T cells. Additionally, we showed that non-cytotoxic T_{FH} cells exhibit a stem-like progenitor exhaustion phenotype with high TCF1 and low BLIMP1/LAG-3 expression and that T_{FH}-like cytotoxic $CD4^+$ T cells exhibit a terminally differentiated exhaustion phenotype with low TCF1 and high BLIMP1/LAG-3 expression, which has been reported in $CD8^+$ T cell exhaustion. Our findings provide deep insights into cancer-specific T_{FH}-like $CD4^+$ T cell exhaustion with helper progenitor and cytotoxic differentiated functions, which mediate anti-tumor immunity orchestrally with cancer-specific exhausted $CD8^+$ T cells.

Limitations of the study

One limitation is the small sample size of the scRNA-seq. Thus, we confirmed these gradient cytotoxic and non-cytotoxic T_{FH}-like $CD4^+$ T cell populations using publicly available datasets (melanoma, lung cancer, and colorectal cancer), whereas MHC-II expression in tumors may be unknown in these cohorts.[27,28] In addition, we obtained paired samples from only one patient before and after anti-PD-1 mAb administration. Although our gating of T_{FH} cells was based on isotype controls and similar to that of another previous study,[17] the gating strategy using PD-1 and CXCR5 in mouse models was somewhat unconvincing. Also, all our panels include live/dead and CD3 staining, which indicates that they accurately identified living $CD3^+$ T cells (Figure S3A), but the possibility of other immune cell contamination such as CXCR5 high B cells has not been completely ruled out. We used *Bcl6*$^{fl/fl}$*Cd4*^{cre} mice for T_{FH} cell knockout, but *Bcl6* deletion also reportedly affects effector $CD4^+$ T cells.[31] Although $CD44^+CD62L^-CD4^+$ effector T cells were comparable, TCF1 expression in $CD4^+$ T cells decreased in these mice, which might be related to the unexpected results.

STAR★METHODS

Detailed methods are provided in the online version of this paper and include the following:

- KEY RESOURCES TABLE
- RESOURCE AVAILABILITY
  - Lead contact
  - Materials availability
  - Data and code availability
- EXPERIMENTAL MODEL AND SUBJECT DETAILS
  - Patients and samples
  - Cell lines
  - Mouse models
- METHOD DETAILS
  - scRNA/TCR-seq
  - Data analysis for scRNA/TCR-seq
  - RNA velocity
  - Diffusion map analysis
  - Publicly available dataset analysis
  - Constructs
  - Virus production and transfection
  - Mouse *B2m*-deletion and human TCR-deletion using CRISPR/Cas9 technology
  - *In vitro* assays for human PBMCs
  - Gene expression analysis
  - Luciferase reporter assay for cancer specificity
  - Killing assay
  - *Ex vivo* assays of T_{FH} cells
  - *In vitro* transduction and analyses for T_{FH} cells from mouse splenocytes
  - Mouse TCR sequencing and data analyses
  - Flow cytometry analysis
- QUANTIFICATION AND STATISTICAL ANALYSIS

SUPPLEMENTAL INFORMATION

Supplemental information can be found online at https://doi.org/10.1016/j.celrep.2024.113797.

ACKNOWLEDGMENTS

We thank Ms. E. Tanji, N. Sakurai, R. Inukai, M. Iwado, Y. Nishimori, S. Nakada, and the Central Research Laboratory in Okayama University Medical School

for their technical assistance. This study was supported by Grants-in-Aid for Scientific Research (Challenging Exploratory Research no. 22K1945904 to Y.T., S grant no. 21H05051 to Y.T., B grant no. 20H03694 to Y.T., C grant no. 19K08744 to T. Inozume., Research Activity Start-up no. 22K20824 to J.N., Early-Career Scientists no. 22K15472 to Y.U., and no. 23K14594 to J.N.) from Japan Society for the Promotion of Science (JSPS); the Project for Cancer Research and Therapeutic Evolution (P-CREATE, no. 19cm0106502 to M.K. and no. 21cm0106383 to K.Y. and Y.T.); the Practical Research for Innovative Cancer Control (no. 19ck0106521h0001 to K.Y. and Y.T. and no. 22ck0106775h0001 to J.N.); the Core Research for Evolutional Science and Technology (CREST, no. 22gm1810002s0101 to Y.T.) from the Japan Agency for Medical Research and Development (AMED); the Fusion Oriented Research for disruptive Science and Technology (FOREST) (no. 21-211033868 to Y.T.) from Japan Science and Technology Agency (JST); the Naito Foundation (to J.N. and Y.T.); the Astellas Foundation for Research on Metabolic Disorders (to Y.T.); the Wesco Foundation (to Y.T.); the Uehara Memorial Foundation (to J.N. and Y.T.); the Senri Life Science Foundation (to Y.T.); the Relay for Life Japan Cancer Society Foundation (to Y.T.); the Japan Research Foundation for Clinical Pharmacology (to Y.T.); the Takeda Science Foundation (to J.N.); the Kowa Life Science Foundation (to J.N.); the Chugai Foundation for Innovative Drug Discovery Science (to J.N.); the Yasuda Medical Foundation (to J.N.); and the SGH Foundation (to J.N.). This study was partially supported by KOTAI Biotechnologies, Inc.

AUTHOR CONTRIBUTIONS

Conceptualization, Y.T.; methodology, W.Z. and S.K.; T. Ishino, K.K., T.K., Y.U., T.W., H.D., M.K., T. Inozume, J.N., and Y.T.; investigation, W.Z., S.K., T. Ishino, K.K., Y.U., K.Y., M.K., Y.S., H.N., T. Inozume, J.N., and Y.T.; writing – original draft and review & editing, W.Z., S.K., Y.U., M.K., Y.S., H.N., T. Inozume, J.N., and Y.T.; and funding acquisition, M.K., H.N., T. Inozume, and Y.T.

DECLARATION OF INTERESTS

K.Y. is an employee of KOTAI Biotechnologies Inc. M.K. received honoraria from Pacific Biosciences outside of this study. H.N. received honoraria from AstraZeneca, Eisai, and Amjen; honoraria and research funding from Ono Pharmaceutical, Chugai Pharmaceutical, MSD, and Bristol-Myers Squibb; and research funding from Daiichi-Sankyo, Debiopharm Group, Fujifilm, Astellas Pharmaceutical, Bayer Yakuhin, Rakuten Medical, Hitachi, Janssen Research & Development, and BD Japan outside of this study. T. Inozume received honoraria and research grants from Ono Pharmaceutical, Bristol-Myers Squibb, and MSD outside of this study. Y.T. received a research grant from KOTAI Biotechnologies Inc. related to this study; received research grants and honoraria from Ono Pharmaceutical, Bristol-Myers Squibb, AstraZeneca, and Chugai Pharmaceutical; and received research grants from Daiichi-Sankyo, Janssen Pharma, and KORTUC and honoraria from MSD outside of this study.

Received: November 29, 2022
Revised: March 13, 2023
Accepted: February 1, 2024

REFERENCES

1. Zou, W., Wolchok, J.D., and Chen, L. (2016). PD-L1 (B7-H1) and PD-1 pathway blockade for cancer therapy: Mechanisms, response biomarkers, and combinations. Sci. Transl. Med. *8*, 328rv4, 328rv324. https://doi.org/10.1126/scitranslmed.aad7118.
2. Topalian, S.L., Drake, C.G., and Pardoll, D.M. (2015). Immune checkpoint blockade: a common denominator approach to cancer therapy. Cancer Cell *27*, 450–461. https://doi.org/10.1016/j.ccell.2015.03.001.
3. Brahmer, J.R., Tykodi, S.S., Chow, L.Q.M., Hwu, W.J., Topalian, S.L., Hwu, P., Drake, C.G., Camacho, L.H., Kauh, J., Odunsi, K., et al. (2012). Safety and activity of anti-PD-L1 antibody in patients with advanced cancer. N. Engl. J. Med. *366*, 2455–2465. https://doi.org/10.1056/NEJMoa1200694.
4. Topalian, S.L., Hodi, F.S., Brahmer, J.R., Gettinger, S.N., Smith, D.C., McDermott, D.F., Powderly, J.D., Carvajal, R.D., Sosman, J.A., Atkins, M.B., et al. (2012). Safety, activity, and immune correlates of anti-PD-1 antibody in cancer. N. Engl. J. Med. *366*, 2443–2454. https://doi.org/10.1056/NEJMoa1200690.
5. Schaerli, P., Willimann, K., Lang, A.B., Lipp, M., Loetscher, P., and Moser, B. (2000). CXC chemokine receptor 5 expression defines follicular homing T cells with B cell helper function. J. Exp. Med. *192*, 1553–1562. https://doi.org/10.1084/jem.192.11.1553.
6. Breitfeld, D., Ohl, L., Kremmer, E., Ellwart, J., Sallusto, F., Lipp, M., and Förster, R. (2000). Follicular B helper T cells express CXC chemokine receptor 5, localize to B cell follicles, and support immunoglobulin production. J. Exp. Med. *192*, 1545–1552. https://doi.org/10.1084/jem.192.11.1545.
7. Crotty, S. (2019). T Follicular Helper Cell Biology: A Decade of Discovery and Diseases. Immunity *50*, 1132–1148. https://doi.org/10.1016/j.immuni.2019.04.011.
8. Qi, H. (2016). T follicular helper cells in space-time. Nat. Rev. Immunol. *16*, 612–625. https://doi.org/10.1038/nri.2016.94.
9. Hollern, D.P., Xu, N., Thennavan, A., Glodowski, C., Garcia-Recio, S., Mott, K.R., He, X., Garay, J.P., Carey-Ewend, K., Marron, D., et al. (2019). B Cells and T Follicular Helper Cells Mediate Response to Checkpoint Inhibitors in High Mutation Burden Mouse Models of Breast Cancer. Cell *179*, 1191–1206.e21. https://doi.org/10.1016/j.cell.2019.10.028.
10. Zhang, Y., Chen, H., Mo, H., Hu, X., Gao, R., Zhao, Y., Liu, B., Niu, L., Sun, X., Yu, X., et al. (2021). Single-cell analyses reveal key immune cell subsets associated with response to PD-L1 blockade in triple-negative breast cancer. Cancer Cell *39*, 1578–1593.e8. https://doi.org/10.1016/j.ccell.2021.09.010.
11. Gu-Trantien, C., Loi, S., Garaud, S., Equeter, C., Libin, M., de Wind, A., Ravoet, M., Le Buanec, H., Sibille, C., Manfouo-Foutsop, G., et al. (2013). CD4$^+$ follicular helper T cell infiltration predicts breast cancer survival. J. Clin. Invest. *123*, 2873–2892. https://doi.org/10.1172/JCI67428.
12. Helmink, B.A., Reddy, S.M., Gao, J., Zhang, S., Basar, R., Thakur, R., Yizhak, K., Sade-Feldman, M., Blando, J., Han, G., et al. (2020). B cells and tertiary lymphoid structures promote immunotherapy response. Nature *577*, 549–555. https://doi.org/10.1038/s41586-019-1922-8.
13. Cabrita, R., Lauss, M., Sanna, A., Donia, M., Skaarup Larsen, M., Mitra, S., Johansson, I., Phung, B., Harbst, K., Vallon-Christersson, J., et al. (2020). Tertiary lymphoid structures improve immunotherapy and survival in melanoma. Nature *577*, 561–565. https://doi.org/10.1038/s41586-019-1914-8.
14. Petitprez, F., de Reyniès, A., Keung, E.Z., Chen, T.W.W., Sun, C.M., Calderaro, J., Jeng, Y.M., Hsiao, L.P., Lacroix, L., Bougoüin, A., et al. (2020). B cells are associated with survival and immunotherapy response in sarcoma. Nature *577*, 556–560. https://doi.org/10.1038/s41586-019-1906-8.
15. Schumacher, T.N., and Thommen, D.S. (2022). Tertiary lymphoid structures in cancer. Science *375*, eabf9419. https://doi.org/10.1126/science.abf9419.
16. Sautès-Fridman, C., Petitprez, F., Calderaro, J., and Fridman, W.H. (2019). Tertiary lymphoid structures in the era of cancer immunotherapy. Nat. Rev. Cancer *19*, 307–325. https://doi.org/10.1038/s41568-019-0144-6.
17. Niogret, J., Berger, H., Rebe, C., Mary, R., Ballot, E., Truntzer, C., Thibaudin, M., Derangère, V., Hibos, C., Hampe, L., et al. (2021). Follicular helper-T cells restore CD8$^+$-dependent antitumor immunity and anti-PD-L1/PD-1 efficacy. J. Immunother. Cancer *9*, e002157. https://doi.org/10.1136/jitc-2020-002157.
18. Cui, C., Wang, J., Fagerberg, E., Chen, P.M., Connolly, K.A., Damo, M., Cheung, J.F., Mao, T., Askari, A.S., Chen, S., et al. (2021). Neoantigen-driven B cell and CD4 T follicular helper cell collaboration promotes

anti-tumor CD8 T cell responses. Cell *184*, 6101–6118.e13. https://doi.org/10.1016/j.cell.2021.11.007.

19. Kumagai, S., Togashi, Y., Kamada, T., Sugiyama, E., Nishinakamura, H., Takeuchi, Y., Vitaly, K., Itahashi, K., Maeda, Y., Matsui, S., et al. (2020). The PD-1 expression balance between effector and regulatory T cells predicts the clinical efficacy of PD-1 blockade therapies. Nat. Immunol. *21*, 1346–1358. https://doi.org/10.1038/s41590-020-0769-3.

20. Nagasaki, J., Inozume, T., Sax, N., Ariyasu, R., Ishikawa, M., Yamashita, K., Kawazu, M., Ueno, T., Irie, T., Tanji, E., et al. (2022). PD-1 blockade therapy promotes infiltration of tumor-attacking exhausted T cell clonotypes. Cell Rep. *38*, 110331. https://doi.org/10.1016/j.celrep.2022.110331.

21. Miller, B.C., Sen, D.R., Al Abosy, R., Bi, K., Virkud, Y.V., LaFleur, M.W., Yates, K.B., Lako, A., Felt, K., Naik, G.S., et al. (2019). Subsets of exhausted $CD8^+$ T cells differentially mediate tumor control and respond to checkpoint blockade. Nat. Immunol. *20*, 326–336. https://doi.org/10.1038/s41590-019-0312-6.

22. Siddiqui, I., Schaeuble, K., Chennupati, V., Fuertes Marraco, S.A., Calderon-Copete, S., Pais Ferreira, D., Carmona, S.J., Scarpellino, L., Gfeller, D., Pradervand, S., et al. (2019). Intratumoral $Tcf1^+PD\text{-}1^+CD8^+$ T Cells with Stem-like Properties Promote Tumor Control in Response to Vaccination and Checkpoint Blockade Immunotherapy. Immunity *50*, 195–211.e10. https://doi.org/10.1016/j.immuni.2018.12.021.

23. Yost, K.E., Satpathy, A.T., Wells, D.K., Qi, Y., Wang, C., Kageyama, R., McNamara, K.L., Granja, J.M., Sarin, K.Y., Brown, R.A., et al. (2019). Clonal replacement of tumor-specific T cells following PD-1 blockade. Nat. Med. *25*, 1251–1259. https://doi.org/10.1038/s41591-019-0522-3.

24. Bassez, A., Vos, H., Van Dyck, L., Floris, G., Arijs, I., Desmedt, C., Boeckx, B., Vanden Bempt, M., Nevelsteen, I., Lambein, K., et al. (2021). A single-cell map of intratumoral changes during anti-PD1 treatment of patients with breast cancer. Nat. Med. *27*, 820–832. https://doi.org/10.1038/s41591-021-01323-8.

25. Gide, T.N., Quek, C., Menzies, A.M., Tasker, A.T., Shang, P., Holst, J., Madore, J., Lim, S.Y., Velickovic, R., Wongchenko, M., et al. (2019). Distinct Immune Cell Populations Define Response to Anti-PD-1 Monotherapy and Anti-PD-1/Anti-CTLA-4 Combined Therapy. Cancer Cell *35*, 238–255.e6. https://doi.org/10.1016/j.ccell.2019.01.003.

26. Workel, H.H., Lubbers, J.M., Arnold, R., Prins, T.M., van der Vlies, P., de Lange, K., Bosse, T., van Gool, I.C., Eggink, F.A., Wouters, M.C.A., et al. (2019). A Transcriptionally Distinct CXCL13 (+)CD103(+) CD8 (+) T - cell Population Is Associated with B- cell Recruitment and Neoantigen Load in Human Cancer. Cancer Immunol. Res. *7*, 784–796. https://doi.org/10.1158/2326-6066.CIR-18-0517.

27. Lowery, F.J., Krishna, S., Yossef, R., Parikh, N.B., Chatani, P.D., Zacharakis, N., Parkhurst, M.R., Levin, N., Sindiri, S., Sachs, A., et al. (2022). Molecular signatures of antitumor neoantigen-reactive T cells from metastatic human cancers. Science *375*, 877–884. https://doi.org/10.1126/science.abl5447.

28. Hanada, K.I., Zhao, C., Gil-Hoyos, R., Gartner, J.J., Chow-Parmer, C., Lowery, F.J., Krishna, S., Prickett, T.D., Kivitz, S., Parkhurst, M.R., et al. (2022). A phenotypic signature that identifies neoantigen-reactive T cells in fresh human lung cancers. Cancer Cell *40*, 479–493.e6. https://doi.org/10.1016/j.ccell.2022.03.012.

29. Thommen, D.S., Koelzer, V.H., Herzig, P., Roller, A., Trefny, M., Dimeloe, S., Kiialainen, A., Hanhart, J., Schill, C., Hess, C., et al. (2018). A transcriptionally and functionally distinct $PD\text{-}1^+CD8^+$ T cell pool with predictive potential in non-small-cell lung cancer treated with PD-1 blockade. Nat. Med. *24*, 994–1004. https://doi.org/10.1038/s41591-018-0057-z.

30. Tietscher, S., Wagner, J., Anzeneder, T., Langwieder, C., Rees, M., Sobottka, B., de Souza, N., and Bodenmiller, B. (2023). A comprehensive single-cell map of T cell exhaustion-associated immune environments in human breast cancer. Nat. Commun. *14*, 98. https://doi.org/10.1038/s41467-41022-35238-w.

31. Xia, Y., Sandor, K., Pai, J.A., Daniel, B., Raju, S., Wu, R., Hsiung, S., Qi, Y., Yangdon, T., Okamoto, M., et al. (2022). BCL6-dependent TCF-1 + progenitor cells maintain effector and helper CD4 + T cell responses to persistent antigen. Immunity *55*, 1200–1215.e6. https://doi.org/10.1016/j.immuni.2022.05.003.

32. Blank, C.U., Haining, W.N., Held, W., Hogan, P.G., Kallies, A., Lugli, E., Lynn, R.C., Philip, M., Rao, A., Restifo, N.P., et al. (2019). Defining 'T cell exhaustion. Nat. Rev. Immunol. *19*, 665–674. https://doi.org/10.1038/s41577-019-0221-9.

33. Budimir, N., Thomas, G.D., Dolina, J.S., and Salek-Ardakani, S. (2021). Reversing T-cell Exhaustion in Cancer: Lessons Learned from PD-1/PD-L1 Immune Checkpoint Blockade. Cancer Immunol. Res. CIR-21-0515. https://doi.org/10.1158/2326-6066.

34. Schumacher, T.N., and Schreiber, R.D. (2015). Neoantigens in cancer immunotherapy. Science *348*, 69–74. https://doi.org/10.1126/science.aaa4971.

35. Matsushita, H., Vesely, M.D., Koboldt, D.C., Rickert, C.G., Uppaluri, R., Magrini, V.J., Arthur, C.D., White, J.M., Chen, Y.-S., Shea, L.K., et al. (2012). Cancer exome analysis reveals a T-cell-dependent mechanism of cancer immunoediting. Nature *482*, 400–404. https://doi.org/10.1038/nature10755.

36. Rizvi, N.A., Hellmann, M.D., Snyder, A., Kvistborg, P., Makarov, V., Havel, J.J., Lee, W., Yuan, J., Wong, P., Ho, T.S., et al. (2015). Cancer immunology. Mutational landscape determines sensitivity to PD-1 blockade in non-small cell lung cancer. Science *348*, 124–128. https://doi.org/10.1126/science.aaa1348.

37. Rooney, M.S., Shukla, S.A., Wu, C.J., Getz, G., and Hacohen, N. (2015). Molecular and Genetic Properties of Tumors Associated with Local Immune Cytolytic Activity. Cell *160*, 48–61. https://doi.org/10.1016/j.cell.2014.12.033.

38. Diebold, S.S., Cotten, M., Koch, N., and Zenke, M. (2001). MHC class II presentation of endogenously expressed antigens by transfected dendritic cells. Gene Ther. *8*, 487–493. https://doi.org/10.1038/sj.gt.3301433.

39. Emerson, R.O., DeWitt, W.S., Vignali, M., Gravley, J., Hu, J.K., Osborne, E.J., Desmarais, C., Klinger, M., Carlson, C.S., Hansen, J.A., et al. (2017). Immunosequencing identifies signatures of cytomegalovirus exposure history and HLA-mediated effects on the T cell repertoire. Nat. Genet. *49*, 659–665. https://doi.org/10.1038/ng.3822.

40. Khan, O., Giles, J.R., McDonald, S., Manne, S., Ngiow, S.F., Patel, K.P., Werner, M.T., Huang, A.C., Alexander, K.A., Wu, J.E., et al. (2019). TOX transcriptionally and epigenetically programs $CD8^+$ T cell exhaustion. Nature *571*, 211–218. https://doi.org/10.1038/s41586-019-1325-x.

41. Xin, G., Schauder, D.M., Lainez, B., Weinstein, J.S., Dai, Z., Chen, Y., Esplugues, E., Wen, R., Wang, D., Parish, I.A., et al. (2015). A Critical Role of IL-21-Induced BATF in Sustaining CD8-T-Cell-Mediated Chronic Viral Control. Cell Rep. *13*, 1118–1124. https://doi.org/10.1016/j.celrep.2015.09.069.

42. Veatch, J.R., Lee, S.M., Shasha, C., Singhi, N., Szeto, J.L., Moshiri, A.S., Kim, T.S., Smythe, K., Kong, P., Fitzgibbon, M., et al. (2022). Neoantigen-specific $CD4^+$ T cells in human melanoma have diverse differentiation states and correlate with $CD8^+$ T cell, macrophage, and B cell function. Cancer Cell *40*, 393–409.e9. https://doi.org/10.1016/j.ccell.2022.03.006.

43. Meckiff, B.J., Ramírez-Suástegui, C., Fajardo, V., Chee, S.J., Kusnadi, A., Simon, H., Eschweiler, S., Grifoni, A., Pelosi, E., Weiskopf, D., et al. (2020). Imbalance of Regulatory and Cytotoxic SARS-CoV-2-Reactive $CD4^+$ T Cells in COVID-19. Cell *183*, 1340–1353.e16. https://doi.org/10.1016/j.cell.2020.10.001.

44. Xie, M.M., Fang, S., Chen, Q., Liu, H., Wan, J., and Dent, A.L. (2019). Follicular regulatory T cells inhibit the development of granzyme B-expressing follicular helper T cells. JCI Insight *4*, e128076. https://doi.org/10.1172/jci.insight.128076.

45. Chaurio, R.A., Anadon, C.M., Lee Costich, T., Payne, K.K., Biswas, S., Harro, C.M., Moran, C., Ortiz, A.C., Cortina, C., Rigolizzo, K.E., et al. (2022). TGF-β-mediated silencing of genomic organizer SATB1 promotes

Tfh cell differentiation and formation of intra-tumoral tertiary lymphoid structures. Immunity *55*, 115–128.e119. https://doi.org/10.1016/j.immuni.2021.12.007.

46. Quezada, S.A., Simpson, T.R., Peggs, K.S., Merghoub, T., Vider, J., Fan, X., Blasberg, R., Yagita, H., Muranski, P., Antony, P.A., et al. (2010). Tumor-reactive CD4(+) T cells develop cytotoxic activity and eradicate large established melanoma after transfer into lymphopenic hosts. J. Exp. Med. *207*, 637–650. https://doi.org/10.1084/jem.20091918.
47. Xie, Y., Akpinarli, A., Maris, C., Hipkiss, E.L., Lane, M., Kwon, E.K.M., Muranski, P., Restifo, N.P., and Antony, P.A. (2010). Naive tumor-specific CD4(+) T cells differentiated in vivo eradicate established melanoma. J. Exp. Med. *207*, 651–667. https://doi.org/10.1084/jem.20091921.
48. Śledzińska, A., Vila de Mucha, M., Bergerhoff, K., Hotblack, A., Demane, D.F., Ghorani, E., Akarca, A.U., Marzolini, M.A.V., Solomon, I., Vargas, F.A., et al. (2020). Regulatory T Cells Restrain Interleukin-2- and Blimp-1-Dependent Acquisition of Cytotoxic Function by CD4. Immunity *52*, 151–166.e156. https://doi.org/10.1016/j.immuni.2019.12.007.
49. Nagasaki, J., Togashi, Y., Sugawara, T., Itami, M., Yamauchi, N., Yuda, J., Sugano, M., Ohara, Y., Minami, Y., Nakamae, H., et al. (2020). The critical role of CD4+ T cells in PD-1 blockade against MHC-II-expressing tumors such as classic Hodgkin lymphoma. Blood Adv. *4*, 4069–4082. https://doi.org/10.1182/bloodadvances.2020002098.
50. Oh, D.Y., Kwek, S.S., Raju, S.S., Li, T., McCarthy, E., Chow, E., Aran, D., Ilano, A., Pai, C.C.S., Rancan, C., et al. (2020). Intratumoral $CD4^+$ T Cells Mediate Anti-tumor Cytotoxicity in Human Bladder Cancer. Cell *181*, 1612–1625.e13. https://doi.org/10.1016/j.cell.2020.05.017.
51. Takeuchi, A., Badr, M.E.S.G., Miyauchi, K., Ishihara, C., Onishi, R., Guo, Z., Sasaki, Y., Ike, H., Takumi, A., Tsuji, N.M., et al. (2016). CRTAM determines the CD4+ cytotoxic T lymphocyte lineage. J. Exp. Med. *213*, 123–138. https://doi.org/10.1084/jem.20150519.
52. Weiskopf, D., Bangs, D.J., Sidney, J., Kolla, R.V., De Silva, A.D., de Silva, A.M., Crotty, S., Peters, B., and Sette, A. (2015). Dengue virus infection elicits highly polarized CX3CR1+ cytotoxic CD4+ T cells associated with protective immunity. Proc. Natl. Acad. Sci. USA *112*, E4256–E4263. https://doi.org/10.1073/pnas.1505956112.
53. Naito, T., Tanaka, H., Naoe, Y., and Taniuchi, I. (2011). Transcriptional control of T-cell development. Int. Immunol. *23*, 661–668. https://doi.org/10.1093/intimm/dxr078.
54. Donnarumma, T., Young, G.R., Merkenschlager, J., Eksmond, U., Bongard, N., Nutt, S.L., Boyer, C., Dittmer, U., Le-Trilling, V.T.K., Trilling, M., et al. (2016). Opposing Development of Cytotoxic and Follicular Helper CD4 T Cells Controlled by the TCF-1-Bcl6 Nexus. Cell Rep. *17*, 1571–1583. https://doi.org/10.1016/j.celrep.2016.10.013.
55. Choi, Y.S., Gullicksrud, J.A., Xing, S., Zeng, Z., Shan, Q., Li, F., Love, P.E., Peng, W., Xue, H.H., and Crotty, S. (2015). LEF-1 and TCF-1 orchestrate T(FH) differentiation by regulating differentiation circuits upstream of the transcriptional repressor Bcl6. Nat. Immunol. *16*, 980–990. https://doi.org/10.1038/ni.3226.
56. Johnston, R.J., Poholek, A.C., DiToro, D., Yusuf, I., Eto, D., Barnett, B., Dent, A.L., Craft, J., and Crotty, S. (2009). Bcl6 and Blimp-1 are reciprocal and antagonistic regulators of T follicular helper cell differentiation. Science *325*, 1006–1010. https://doi.org/10.1126/science.1175870.
57. Wu, T., Shin, H.M., Moseman, E.A., Ji, Y., Huang, B., Harly, C., Sen, J.M., Berg, L.J., Gattinoni, L., McGavern, D.B., and Schwartzberg, P.L. (2015). TCF1 Is Required for the T Follicular Helper Cell Response to Viral Infection. Cell Rep. *12*, 2099–2110. https://doi.org/10.1016/j.celrep.2015.08.049.
58. Duhen, R., Fesneau, O., Samson, K.A., Frye, A.K., Beymer, M., Rajamanickam, V., Ross, D., Tran, E., Bernard, B., Weinberg, A.D., and Duhen, T. (2022). PD-1 and ICOS coexpression identifies tumor-reactive CD4+ T cells in human solid tumors. J. Clin. Invest. *132*, e156821. https://doi.org/10.1172/JCI156821.
59. Wherry, E.J., and Kurachi, M. (2015). Molecular and cellular insights into T cell exhaustion. Nat. Rev. Immunol. *15*, 486–499. https://doi.org/10.1038/nri3862.
60. Miggelbrink, A.M., Jackson, J.D., Lorrey, S.J., Srinivasan, E.S., Waibl-Polania, J., Wilkinson, D.S., and Fecci, P.E. (2021). CD4 T-Cell Exhaustion: Does It Exist and What Are Its Roles in Cancer? Clin. Cancer Res. *27*, 5742–5752. https://doi.org/10.1158/1078-0432.CCR-21-0206.
61. Nagasaki, J., and Togashi, Y. (2022). A variety of 'exhausted' T cells in the tumor microenvironment. Int. Immunol. *34*, 563–570. https://doi.org/10.1093/intimm/dxac013.
62. Axelrod, M.L., Cook, R.S., Johnson, D.B., and Balko, J.M. (2019). Biological Consequences of MHC-II Expression by Tumor Cells in Cancer. Clin. Cancer Res. *25*, 2392–2402. https://doi.org/10.1158/1078-0432.CCR-18-3200.
63. Tawbi, H.A., Schadendorf, D., Lipson, E.J., Ascierto, P.A., Matamala, L., Castillo Gutiérrez, E., Rutkowski, P., Gogas, H.J., Lao, C.D., De Menezes, J.J., et al. (2022). Relatlimab and Nivolumab versus Nivolumab in Untreated Advanced Melanoma. N. Engl. J. Med. *386*, 24–34. https://doi.org/10.1056/NEJMoa2109970.
64. Landau, N.R., Warton, M., and Littman, D.R. (1988). The envelope glycoprotein of the human immunodeficiency virus binds to the immunoglobulin-like domain of CD4. Nature *334*, 159–162. https://doi.org/10.1038/334159a0.
65. Dull, T., Zufferey, R., Kelly, M., Mandel, R.J., Nguyen, M., Trono, D., and Naldini, L. (1998). A third-generation lentivirus vector with a conditional packaging system. J. Virol. *72*, 8463–8471. https://doi.org/10.1128/jvi.72.11.8463-8471.1998.
66. Morgenstern, J.P., and Land, H. (1990). Advanced mammalian gene transfer: high titre retroviral vectors with multiple drug selection markers and a complementary helper-free packaging cell line. Nucleic Acids Res. *18*, 3587–3596. https://doi.org/10.1093/nar/18.12.3587.
67. Hafemeister, C., and Satija, R. (2019). Normalization and variance stabilization of single-cell RNA-seq data using regularized negative binomial regression. Genome Biol. *20*, 296. https://doi.org/10.1186/s13059-019-1874-1.
68. La Manno, G., Soldatov, R., Zeisel, A., Braun, E., Hochgerner, H., Petukhov, V., Lidschreiber, K., Kastriti, M.E., Lönnerberg, P., Furlan, A., et al. (2018). RNA velocity of single cells. Nature *560*, 494–498. https://doi.org/10.1038/s41586-018-0414-6.
69. Wolf, F.A., Angerer, P., and Theis, F.J. (2018). SCANPY: large-scale single-cell gene expression data analysis. Genome Biol. *19*, 15. https://doi.org/10.1186/s13059-017-1382-0.
70. Bergen, V., Lange, M., Peidli, S., Wolf, F.A., and Theis, F.J. (2020). Generalizing RNA velocity to transient cell states through dynamical modeling. Nat. Biotechnol. *38*, 1408–1414. https://doi.org/10.1038/s41587-020-0591-3.
71. Dobin, A., Davis, C.A., Schlesinger, F., Drenkow, J., Zaleski, C., Jha, S., Batut, P., Chaisson, M., and Gingeras, T.R. (2013). STAR: ultrafast universal RNA-seq aligner. Bioinformatics *29*, 15–21. https://doi.org/10.1093/bioinformatics/bts635.
72. Li, B., and Dewey, C.N. (2011). RSEM: accurate transcript quantification from RNA-Seq data with or without a reference genome. BMC Bioinf. *12*, 323. https://doi.org/10.1186/1471-2105-12-323.
73. Robin, X., Turck, N., Hainard, A., Tiberti, N., Lisacek, F., Sanchez, J.C., and Müller, M. (2011). pROC: an open-source package for R and S+ to analyze and compare ROC curves. BMC Bioinf. *12*, 77. https://doi.org/10.1186/1471-2105-12-77.
74. Bolotin, D.A., Poslavsky, S., Mitrophanov, I., Shugay, M., Mamedov, I.Z., Putintseva, E.V., and Chudakov, D.M. (2015). MiXCR: software for comprehensive adaptive immunity profiling. Nat. Methods *12*, 380–381. https://doi.org/10.1038/nmeth.3364.

STAR★METHODS

KEY RESOURCES TABLE

REAGENT or RESOURCE	SOURCE	IDENTIFIER
Antibodies		
Anti-human HLA-DR,DP,DQ-PE-Cy7 (Tü39)	Biolegend	Cat# 361708; RRID:AB_2564279
Anti-human CD3-AF700 (UCHT1)	Biolegend	Cat# 300424; RRID:AB_493741
Anti-human CD4-BV510 (SK3)	BD Biosciences	Cat# 562970; RRID:AB_2744424
Anti-human CD8-FITC (RPA-T8)	Biolegend	Cat# 301006; RRID:AB_314124
Anti-human CD185-APC (J252D4)	Biolegend	Cat# 356907; RRID:AB_2561816
Anti-human CD279-BV421 (MIH4)	BD Biosciences	Cat# 564323; RRID:AB_2738745
Anti-human CXCL13-PE (53610)	Thermo Fisher Scientific	Cat# MA5-23666; RRID:AB_2610226
Anti-human TCR$\alpha\beta$-FITC (IP26)	Biolegend	Cat# 306706; RRID:AB_314644
Anti-mouse CD3-V500 (500A2)	BD Biosciences	Cat# 560771; RRID:AB_1937314
Anti-mouse CD3-Alexa Fluor 700 (500A2)	BD Biosciences	Cat# 557984; RRID:AB_396972
Anti-mouse CD3-APC-Cy7 (17A2)	Biolegend	Cat# 100222; RRID:AB_2242784
Anti-mouse CD4-PE-Cy7 (RM4-5)	BD Biosciences	Cat# 552775; RRID:AB_394461
Anti-mouse CD4-PE-Cy5 (GK1.5)	Biolegend	Cat# 100409; RRID:AB_312694
Anti-mouse CD4-PerCP-Cy5.5 (RM4-5)	BD Biosciences	Cat# 550954; RRID:AB_393977
Anti-mouse CD8a-PerCP-Cy5.5 (53–6.7)	BD Biosciences	Cat# 551162; RRID:AB_394081
Anti-mouse CD44-BV510 (IM7)	BD Biosciences	Cat# 563114; RRID:AB_2738011
Anti-mouse CD62L-PE (MEL-14)	BD Biosciences	Cat# 553151; RRID:AB_394666
Anti-mouse CD62L-PE-Cy5 (MEL-14)	Biolegend	Cat# 104410 RRID:AB_313097
Anti-mouse CD279 (PD-1)-BV421 (29F.1A12)	Biolegend	Cat# 135217; RRID:AB_10900085
Anti-mouse CD279 (PD-1)-APC (29F.1A12)	Biolegend	Cat# 135210; RRID:AB_2159183
Anti-mouse CD279 (PD-1)-PE-Cy7 (29F.1A12)	Biolegend	Cat# 135215; RRID:AB_10696422
Anti-mouse Granzyme B-PE (QA16A02)	Biolegend	Cat# 372208; RRID:AB_2687032
Anti-mouse Granzyme B-PerCp-Cy5.5 (QA16A02)	Biolegend	Cat# 372211; RRID:AB_2728378
Anti-mouse Perforin-APC (S16009B)	Biolegend	Cat# 154403; RRID:AB_2721464
Anti-mouse CXCL13-APC (DS8CX13)	Thermo Fisher Scientific	Cat# 17-7981-80; RRID:AB_2762702
Anti-mouse CD185 (CXCR5)-FITC (L138D7)	Biolegend	Cat# 145520; RRID:AB_2562866
Anti-mouse CD183 (CXCR3)-PE (CXCR3-173)	Biolegend	Cat# 126506; RRID:AB_1027650
Anti-mouse Bcl-6-PE (7D1)	Biolegend	Cat# 358504; RRID:AB_2562152
Anti-mouse Bcl-6-PerCP-Cy5.5 (K112-91)	BD Biosciences	Cat# 562198; RRID:AB_11153136
Anti-mouse TCF-7-Alexa Fluor 647 (S33-966)	BD Biosciences	Cat# 566693; RRID:AB_2869823
Anti-mouse Blimp-1-BV421 (5E7)	BD Biosciences	Cat# 564270; RRID:AB_2738720
Anti-mouse GATA3-PE (16E10A23)	Biolegend	Cat# 653803 RRID:AB_2562722
Anti-T-bet Antibody-BV605 (4B10)	Biolegend	Cat# 644817 RRID: AB_11219388
Anti-mouse CD223-BV711 (C9B7W)	BD Biosciences	Cat# 563179; RRID:AB_2737398
Anti-mouse CD223-APC (C9B7W)	BD Biosciences	Cat# 562346; RRID:AB_11153127
Anti-mouse FoxP3-PE-CF594 (R16-715)	BD Biosciences	Cat# 567373; RRID:AB_2916572
Anti-mouse TOX-PE (TXRX10)	eBioscience	Cat# 12-6502-80; RRID:AB_10853657
Anti-mouse CD69-FITC (H1.2F3)	Biolegend	Cat# 104506; RRID:AB_313109
Anti-mouse IFN-γ-BV421 (XMG1.2)	BD Biosciences	Cat# 563376; RRID:AB_2738165
Anti-mouse IFN-γ-APC (XMG1.2)	BD Biosciences	Cat# 554413; RRID:AB_398551

(*Continued on next page*)

Continued

REAGENT or RESOURCE	SOURCE	IDENTIFIER
Anti-mouse TNF-α-BV421 (MP6-XT22)	Biolegend	Cat# 506327; RRID:AB_10900823
Anti-mouse TNF-α-BV605 (MP6-XT22)	Biolegend	Cat# 506329; RRID:AB_11123912
Anti-mouse H-2-PE (M1/42)	Biolegend	Cat# 125508; RRID:AB_1236470
Anti-mouse I-A/I-E-Alexa Flour 488 (M5/114.15.2)	Biolegend	Cat# 107616; RRID:AB_493523
Purified anti-human CD3 (OKT3)	Thermo Fisher Scientific	Cat# 16-0037-81; RRID:AB_468854
Purified anti-human CD28 (CD28.2)	Thermo Fisher Scientific	Cat# 16-0289-85; RRID:AB_468926
Purified anti-human CD3 (145-2C11)	Biolegend	Cat# 100359; RRID:AB_2616673
Purified anti-mouse CD28 (37.51)	Biolegend	Cat# 102116; RRID:AB_11147170
Anti-mouse CD8b (Lyt 3.2) (53–5.8)	Bio X Cell	Cat# BE0223; RRID:AB_2687706
Anti-mouse CXCL13 (143614)	R&D Systems	Cat# MAB470-500; RRID:AB_2086062
Anti-mouse PD-1 (RMP1-14)	Biolegend	Cat# 114111; RRID:AB_2566089
Anti-mouse LAG-3 mAb (C9B7W)	Biolegend	Cat# 125217; RRID:AB_2566284
Purified Rat IgG2a κ isotype control (RTK2758)	Biolegend	Cat# 400502; RRID:AB_326523
Brilliant Violet 421™ Rat IgG2a, κ Isotype Ctrl Antibody	Biolegend	Cat#; 400535 RRID:AB_10933427
FITC Rat IgG2b, κ Isotype Ctrl Antibody	Biolegend	Cat#; 400634 RRID:AB_893662
Fc Receptor Binding Inhibitor Functional Grade Polyclonal Antibody	Thermo Fisher Scientific	Cat# 16-9161-73; RRID:AB_469272
Chemicals, peptides, and recombinant proteins		
Fetal Bovine Serum	Cytiva	Cat# SH30396
RPMI 1640 Medium	Thermo Fisher Scientific	Cat# 11875093
D-MEM Medium	Wako	Cat# 044-29765
Collagenase type IV	Sigma-Aldrich	Cat# C4-28-100MG
Hyaluronidase type V	Sigma-Aldrich	Cat# H6254-500MG
Deoxyribonuclease I type IV	Sigma-Aldrich	Cat# D5025-15KU
Penicillin-streptomycin	Thermo Fisher Scientific	Cat# 14150122
Hygromycin B Solution	nacalai tesque	Cat# 09287-84
Puromycin Dihydrochloride	Wako	Cat# 166-23153
Amphotricin B	Thermo Fisher Scientific	Cat# 15290018
rhIL-2	PeproTech	Cat# 200-02
rhIFN-γ	PeproTech	Cat# AF-300-02
Fixable Viability Dye-eFluor 780	Thermo Fisher Scientific	Cat# 65-0865-14
7-AAD	Thermo Fisher Scientific	Cat# A1310
Calcein-AM	Thermo Fisher Scientific	Cat# C1430
Lymphocyte Separation Solution	NACALAI TESQUE INC	Cat# 20828-15
Critical commercial assays		
Foxp3/Transcription Factor Staining Buffer Set	Thermo Fisher Scientific	Cat# 00-5523-00
Protein Transport Inhibitor (Containing Monensin)	BD Biosciences	Cat# 554724
PCR Mycoplasma Detection Kit	Takara Bio	Cat# CY232
Lipofectamine 3000	Thermo Fisher Scientific	Cat# L3000008
RetroNectin	Takara Bio	Cat# T100B
In-Fusion Snap Assembly Master Mix	Takara Bio	Cat# Z8947N
KOD -Plus- mutagenesis kit	TOYOBO	Cat# SMK-101
TrueCut Cas9 Protein v2	Thermo Fisher Scientific	Cat# A36498
Lipofectamine CRISPRMAX Cas9 Transfection Reagent	Thermo Fisher Scientific	Cat# CMAX00008
RBC Lysis Buffer (10X)	Biolegend	Cat# 420301
MojoSort Mouse CD4 T cell Isolation Kit	Biolegend	Cat# 480005

(*Continued on next page*)

Continued

REAGENT or RESOURCE	SOURCE	IDENTIFIER
Bright-Glo™ Luciferase Assay System	Promega	Cat# E2610
PE Annexin V Apoptosis Detection Kit with 7-AAD	BioLegend	Cat# 640934
CellTrace™ CFSE Cell Proliferation Kit	Thermo Fisher Scientific	Cat# C34554
PrimeScript RT Master Mix	TaKaRa	Cat# RR036A
TB Green Premix Ex Taq II	TaKaRa	Cat# RR820
Deposited data		
Single-cell sequencing for melanoma samples	This paper	DDBJ: JGAS000285
Bulk TCR-sequencing of mice	This paper	DDBJ: DRA016998
Single-cell sequencing for lung cancer samples	Hanada et al.[28]	dbGaP: phs002792.v1.p1
Single-cell sequencing for melanoma, lung cancer, and colorectal cancer samples	Lowery et al.[27]	dbGaP: phs002748.v1.p1
Publicly available bulk RNA-sequencing data for melanoma patients who received anti-PD-1 mAb	Gide et al.[25]	BioProject: PRJEB23709
Experimental models: Cell lines		
MEL02-1	N/A	N/A
MEL02-2	N/A	N/A
MEL03	N/A	N/A
MEL04	N/A	N/A
E.G7	ATCC	Cat# CRL-2113
B16F10	ATCC	Cat# CRL-6475
Jurkat, Clone E6-1	ATCC	Cat# TIB-152
LL/2	ATCC	Cat# CRL-1642
MC-38	Kerafast	Cat# ENH204
Experimental models: Organisms/strains		
C57BL/6	Japan SLC	N/A
B6 SCID	RIKEN BRC	N/A
OT-II	Jackson Laboratories	N/A
CD4Cre	Jackson Laboratories	N/A
BCL6fl	Jackson Laboratories	N/A
Recombinant DNA		
pcDNA3-TfR-OVA	Diebold et al.[38]	Addgene_64600
pMX-hCD4	Landau et al.[64]	Addgene_14614
pMDLg/pRRE	Dull et al.[65]	Addgene_12251
pRSV-REV	Dull et al.[65]	Addgene_12253
pMD2.G	Didier Trono	Addgene_12259
pBABE puro	Morgenstern et al.[66]	Addgene_1764
pMSCV-hCIITA	VectorBuilder	Cat# VB210215-1026npf
pMSCV-hTCRB-hTCRA vector	VectorBuilder	N/A
pLV-mTcf7-EGFP	VectorBuilder	Cat# VB220318-1209zdc
pLV[shRNA]-EGFP-mPrdm1	VectorBuilder	Cat# VB220318-1204rzb
mouse Ciita cDNA	K.K. DNAFORM	Cat# 100015714
pGL4.30 [luc2P/NFAT-RE/Hygro] Luciferase Reporter Vectors	Promega	Cat# 9PIE848
pVSV-G	Takara Bio	Cat# 631530
Oligonucleotides		
sgRNA mouse b2m 5'-TTCGGCTTC CCATTCTCCGG-3'	Thermo Fisher Scientific	Cat# A35533
sgRNA human TCRA 5'-CTCGACC AGCTTGACATCAC-3'	Integrated DNA Technologies	N/A

(*Continued on next page*)

Continued

REAGENT or RESOURCE	SOURCE	IDENTIFIER
sgRNA human TCRB 5'-AGAAGG TGGCCGAGACCCTC-3'	Integrated DNA Technologies	N/A
Human *CXCL13*-Forward (TATCCCTAGACGCTTCATTGATCG)	Eurofins	N/A
Human CXCL13-Reverse (CCATTCAGCTTGAGGGTCCACA)	Eurofins	N/A
Mouse *Cxcl13*-Forward (CATAGATCGGATTCAAGTTACGCC)	Eurofins	N/A
Mouse *Cxcl13*- Reverse (GTAACCATTTGGCACGAGGATTC)	Eurofins	N/A
Human *GAPDH*-Forward (GACTCATGACCACAGTCCATGC)	Eurofins	N/A
Human *GAPDH*-Reverse (GAGGAGACCACCTGGTGCTCAG)	Eurofins	N/A
Mouse *Gapdh*-Forward (CATCACTGCCACCCAGAAGACTG)	Eurofins	N/A
Mouse *Gapdh*-Reverse (ATGCCAGTGAGCTTCCCGTTCAG)	Eurofins	N/A
Other		
FlowJo 10.0.8	BD Biosciences	N/A
GraphPad Prism 8	GraphPad Software Inc.	N/A
R version 4.0.2	R Foundation for Statistical Computing	N/A
Python v3.9.13	Python Software Foundation	N/A

RESOURCE AVAILABILITY

Lead contact

Further information and requests for resources and reagents should be directed to and will be fulfilled by the lead contact, Yosuke Togashi (ytogashi1584@gmail.com).

Materials availability

Plasmids and cell lines generated in this study are available from the lead contact; however, we may require a completed materials transfer agreement.

Data and code availability

- scRNA-seq and scTCR-seq data have been deposited at DDBJ, and they are publicly available as of the date of publication. Accession numbers are listed in the key resources table. Original plate reader measurements and flow cytometry measurements reported in this paper will be shared by the lead contact upon request.
- This paper does not report original code.
- Any additional information required for reanalyzing the data reported in this paper is available from the lead contact upon request.

EXPERIMENTAL MODEL AND SUBJECT DETAILS

Patients and samples

Three patients (all male in their 60s–80s) with melanoma, who underwent surgical resection at Yamanashi University Hospital from 2017 to 2019, were enrolled in this study for establishing autologous cancer cell lines and cultured TILs (Table S1). All patients provided written informed consents before sampling, according to the Declaration of Helsinki. The protocol for this study was approved by the appropriate institutional review board and ethics committees at the Yamanashi University Hospital, Chiba University Hospital, Okayama University Hospital and Chiba Cancer Center.

Tumor specimens were excised aseptically. All resected specimens were obtained for pathologic confirmation of the diagnosis, and we used remaining samples. Surgically resected samples were enzymatically digested with collagenase, hyaluronidase, and deoxyribonuclease (Sigma-Aldrich, St. Louis, MO) in RPMI 1640 (Thermo Fisher Science, Waltham, MA). After filtration and

separation by density gradient using Lymphocyte Separation Solution (NACALAI TESQUE INC, Kyoto, Japan), the digested tumor cells were cryopreserved until use.[20]

Cell lines

For establishing cancer cell lines, 1×10^7 digested tumor cells were cultured in RPMI 1640 containing 10% fetal bovine serum (FBS; Cytiva, Tokyo, Japan), penicillin–streptomycin, and amphotericin B (Thermo Fisher Science). Tumor cells were passaged at approximately 80%–90% confluence and used when free of fibroblasts and proliferated beyond the 10th passage. All patients were responders to anti-PD-1 mAb. The MEL02-1 and MEL02-2 cell lines were generated from the same patient before and during the treatment, respectively.[20]

The E.G7, B16F10, LL/2, and Jurkat cell lines were purchased from ATCC (Manassas, VA; Cat#CRL-2113, RRID: CVCL_3505; Cat#CRL-6475, RRID: CVCL_0159; Cat#CRL-1642, RPID: CVCL_4358; and Cat#TIB-152, RRID: CVCL_0367, respectively). The MC-38 cell line (mouse colon cancer) was purchased from Kerafast (Boston, MA; Cat# ENH204, RRID: CVCL_B288). The E.G7, B16F10, LL/2, and Jurkat cell lines were maintained in RPMI 1640 medium supplemented with 10% FBS, and the MC-38 cell line was maintained in DMEM (Thermo Fisher Science) supplemented with 10% FBS. All cell lines were used after confirming that they were mycoplasma (−) after mycoplasma testing using the PCR Mycoplasma Detection Kit (Takara Bio; Shiga, Japan) according to the manufacturer's protocol.

Mouse models

The following mouse strains were used in this study: Female C57BL/6J mice (6–8 weeks old) were purchased from Japan SLC (Shizuoka, Japan). C57BL/6J-Prkdc<scid>/Rbrc mice (B6 SCID; RBRC01346) were provided by RIKEN BRC (Tsukuba, Japan) through the National BioResource Project of the MEXT/AMED, Japan. B6.Cg-Tg(TcraTcrb)425Cbn/J mice (*OT-II*; IMSR_JAX:004194), B6.Cg-Tg(Cd4-cre)1Cwi/BfluJ mice ($Cd4^{cre}$; IMSR_JAX:022071), and B6.129S(FVB)-Bcl6tm1.1Dent/J mice ($Bcl6^{fl}$; IMSR_JAX:023727) were obtained from Jackson Laboratories (Bar Harbor, ME).

MC-38, B16F10, LL/2 cells, or E.G7 cells (1×10^6 cells) were injected subcutaneously on day 0, and the tumor volume was monitored twice a week. The means of the long and short tumor diameters were used for generating tumor growth curves. The mice were grouped when the tumor volume reached approximately 100 mm^3, and anti-PD-1 mAb (200 μg/mouse) or control mAb was administered intraperitoneally three times every 3 days on day 5. Tumors were harvested on day 5, 14, and 21, or 7 days after treatment initiation for TIL analyses or sorting. When cytotoxicity was evaluated, we stimulated TILs with anti-CD3 and CD28 mAbs (BioLegend; San Diego, CA) for 6 h after harvesting. For CD8 deletion, anti-CD8β mAb (100 μg/mouse) was administered intraperitoneally on days −1 and 6. For CXCL13 blockade, anti-mouse CXCL13 mAb (100 μg/mouse) was administered intraperitoneally three times in a week. Rat anti-mouse PD-1 mAb (RMP1-14) and control mAb (RTK2758) were purchased from BioLegend. An anti-mouse CD8β mAb (53–5.8) was purchased from Bio X Cell (West Lebanon, New Hampshire). An anti-CXCL13 mAb (143614) was purchased from R&D systems (Minneapolis, MI).

For T cell transfer, 1×10^6 MC-38/OVA/B2mKO/mCiita or MC-38/OVA cells were injected subcutaneously in B6 SCID mice on day 0, and 2×10^6 PD-1^+CXCR5^+CD25^-CD4^+ T cells (T_{FH} cells) sorted from *OT-II* splenocytes using FACSMelody or FACSAria (BD Biosciences; San Jose, CA) in Central Research Laboratory, Okayama University Medical School were injected intraperitoneally on days 0, 4, and 10. The means of the long and short tumor diameters were used for generating tumor growth curves.

In vivo experiments were performed at least twice. All animals were bred and housed under specific pathogen-free conditions at the Chiba Cancer Center Research Institute and Okayama University. Mouse experiments were approved by the Animal Committee for Animal Experimentation of the Chiba Cancer Center and Okayama University. All experiments met the U.S. Public Health Service Policy on the Humane Care and Use of Laboratory Animals.

METHOD DETAILS

scRNA/TCR-seq

The libraries for scRNA-seq and scTCR-seq were prepared using the 10x Single-Cell Immune Profiling Solution Kit according to the manufacturer's protocol (10x Technologies Inc., Pleasanton, CA). CD3^+ T cells sorted by FACSAria were washed and resuspended in PBS with 0.5% FBS. Cells were captured in droplets at a targeted cell recovery rate of <10,000 cells. After reverse transcription and cell barcoding in droplets, the emulsions were broken, and the purified cDNA was amplified using Dynabeads MyOne SILANE (Thermo Fisher Scientific), followed by PCR amplification. To construct 5′ gene expression libraries, 2.4–50 ng of amplified cDNA was fragmented, end-repaired, double-sided size-selected with SPRIselect beads (Beckman Coulter, Brea, CA, USA), PCR-amplified with sample indexing primers, and double-sided size-selected with SPRIselect beads. TCR transcripts were enriched from 2 μL of amplified cDNA using PCR to construct TCR libraries. Following enrichment, 5–50 ng of the enriched PCR product was fragmented and end-repaired, size-selected with SPRIselect beads, PCR-amplified with sample indexing primers, and size-selected with SPRIselect beads. We sequenced the scRNA and scTCR libraries using a HiSeq 3000 instrument to a minimum sequencing depth of 25,000 and 5,000 reads per cell, respectively. Sequencing read lengths were adjusted for each library type according to the manufacturer's protocol and the reagent version.[20]

Data analysis for scRNA/TCR-seq

The reads were processed using the CellRanger software (10x Technologies Inc., version 6.0.2). Using UMI count matrices loaded via the Seurat R package (version 4.2.0),[67] cells with a mitochondrial content above 10% and cells with less than 200 or more than 4000 detected genes were filtered out as dying cells, empty droplets, and doublets, respectively. For normalization, the Seurat NormalizeData function was used, which was subsequently integrated using the IntegrateData function. The dimension was reduced by running PCA and then computing the UMAP embeddings using the first 15 components of the PCA for visualization and clustering. Finally, we manually annotated each cluster according to the expression of known marker genes, including *CD3D*, *CD3E*, and *CD2* (T cells); *CD4* and *CCR7* (naive $CD4^+$ T cells); *CD4* and *FOXP3* (T_{reg} cells); *CD4*, *CD200*, and *CXCL13* (T_{FH} cells); *CD4* and *CD69* (activated $CD4^+$ T cells); *CD4*, *CXCR3*, *CCR4*, and *IL7R* (memory $CD4^+$ T cells); *CD8A* and *CD69* (activated $CD8^+$ T cells); *CD8A*, *CXCR3*, *EOMES*, and *IL7R* (memory $CD8^+$ T cells); *CD8A*, *GZMA*, and *PRF1* (effector $CD8^+$ T cells); and *CD8A*, *PDCD1*, and *HAVCR2* (exhausted $CD8^+$ T cells).[20] In addition, exhausted $CD8^+$ T cells, T_{FH} cells, and non-naïve/non-T_{reg} $CD4^+$ T cells were extracted and reclassified. In brief, the dimension was reduced by running PCA and then computing the UMAP embeddings using the first 10 components of the PCA for visualization and clustering. For the T_{FH} cells, we manually annotated the population with high expression of *GZMA*, *GZMB*, *PRF1, CCL4, CCL5,* and *CXCR6* as cytotoxic T_{FH} cells and the other population as non-cytotoxic T_{FH} cells. For non-naïve/non-T_{reg} $CD4^+$ T cells, we manually annotated the populations with high expression of *CXCL13*, *CD200*, *CXCR5*, *GZMA*, and *PRF1* (cytotoxic T_{FH} cells); *CXCL13*, *CD200*, *CXCR5*, and *TCF7* (non-cytotoxic T_{FH} cells); *TCF7* and *CCR7* (progenitor $CD4^+$ T cells); *CD69*, *GZMA*, and *IFNG* (effector $CD4^+$ T cells).

TCR reads were aligned to the GRCh38 reference genome, and cellranger vdj pipeline (10x Technologies, Inc, version 6.0.2) was used for consensus TCR annotation according to the manufacturer's protocol. As matching to public bulk TCR datasets is usually performed at the TCRβ level, cells with no reconstructed TCRα clonotype were retained, while cells with no TCRβ clonotype were not retained for subsequent analysis. The clonotype with the highest number of UMIs was used for cells with two or more clonotypes. If the number of UMIs in the second clonotype was more than half of that in the top clonotype, the cells were labelled as ambiguous.

RNA velocity

We used velocyto v0.17.17 to generate loom files from bam files, which were generated using Cell Ranger.[68] Next, the individual loom files were merged and Harmony-integrated using scanpy v1.8.2 in python v3.9.13.[69] We then ran scVelo v0.2.4 using default settings to obtain RNA velocity and latent time.[70] The RNA velocity (direction and speed of migration) of individual cells were estimated from the ratio of unspliced/spliced in the mRNA count data for each gene.

Diffusion map analysis

We applied a diffusion map as a nonlinear dimensionality reduction technique to examine the major components of variation across different cell types for latent time. We computed Diffusion Components (DCs) using the 'scanpy.tl.diffmap' function of the scanpy v1.8.2 in python v3.9.13.[69]

Publicly available dataset analysis

Bulk RNA-seq public data obtained from melanoma patients who received anti-PD-1 mAb were downloaded from NCBI (BioProject: PRJEB23709).[25] Bulk RNA-seq reads were aligned to the GRCh38 reference genome using STAR v2.7.1.[71] Next, we quantified gene expression levels and calculated TPM values from genome mapping data using RSEM v1.3.3 in R v4.2.0.[72] These data were tied to patient information, and survival curves were plotted for progression free survival (PFS) and overall survival (OS) using survival v3.3.1 (Therneau, T. M. (2020). A Package for Survival Analysis in R. https://CRAN.R-project.org/package=survival). The cut-off value for CXCL13 gene expression was calculated from the receiver operating characteristic (ROC) curve plotted using pROC v1.18.0 in R v4.2.0.[73]

scRNA-seq data for melanoma, lung cancer, and colorectal cancer TILs were downloaded from the dbGaP portal (accession no: phs002792.v1.p1 and phs002748.v1.p1).[27,28] The merged data were analyzed as described in the above section "Data analysis for scRNA/TCR-seq".

Constructs

The following constructs were gifts: pcDNA3-*TfR-OVA*, from Sandra Diebold & Martin Zenke (Addgene plasmid #64600; http://n2t.net/addgene:64600; RRID: Addgene_64600)[38]; pMX-*hCD4*, from Dan Littman (Addgene plasmid #14614; http://n2t.net/addgene:14614; RRID: Addgene_14614)[64]; pBABE-puro, from Hartmut Land & Jay Morgenstern & Bob Weinberg (Addgene plasmid #1764; http://n2t.net/addgene:1764; RRID: Addgene_1764)[66]; pMDLg/pRRE, from Didier Trono (Addgene plasmid #12251; http://n2t.net/addgene:12251; RRID: Addgene_12251)[65]; pRSV-Rev, from Didier Trono (Addgene plasmid #12253; http://n2t.net/addgene:12253; RRID: Addgene_12253)[65]; and pMD2.G, from Didier Trono (Addgene plasmid #12259; http://n2t.net/addgene:12259; RRID: Addgene_12259). *mCiita* cDNA was purchased from DNAFORM (Kanagawa, Japan). pMSCV-*hCIITA* (VB210215-1026npf), pMSCV-*hTCRB-hTCRA*, pLV-*mTcf7-EGFP* (VB220318-1209zdc), and pLV[shRNA]-*EGFP-mPrdm1* (VB220318-1204rzb) vectors were created by VectorBuilder (Chicago, IL). A pGL4.30 [luc2P/NFAT-RE/Hygro] vector was purchased from Promega (Madison, WI).

TfR-OVA or mouse *Ciita* (*mCiita*) cDNA was cloned into the pBABE-puro vector using In-Fusion Snap Assembly Master Mix (Takara Bio) according to the manufacturer's protocol. The OVA epitope presented by MHC-I (OVA-I) or MHC-II (OVA-II) was deleted from the

pBABE-puro-*TfR-OVA* vector using the KOD-Plus-mutagenesis kit (TOYOBO; Osaka, Japan) to obtain pBABE-puro-*TfR-OVA-II* and pBABE-puro-*TfR-OVA-I*, respectively, according to the manufacturer's protocol (Figure S3H). The integrities of *TfR-OVA*, *TfR-OVA-I*, and *TfR-OVA-II* were confirmed by DNA sequencing.

Virus production and transfection

pBABE-puro-*mCiita,* pBABE-puro-*TfR-OVA*, pBABE-puro-*TfR-OVA-I*, pBABE-puro-*TfR-OVA-II*, pMX-*hCD4*, pMSCV-*hCIITA,* or each pMSCV-*hTCRB-hTCRA* vector was transfected with pVSV-G vector (Takara Bio) into packaging cells using Lipofectamine 3000 Reagent (Thermo Fisher Scientific). pLV-*mTcf7-EGFP* or pLV[shRNA]-*EGFP-mPrdm1* vector was transfected with pMDLg/pRRE, pRSV-REV, and pMD2.G into packaging cells using Lipofectamine 3000 Reagent. After 48 h, the supernatant was concentrated and transfected into cells.

MC-38 cell lines transfected with *mCiita*, *TfR-OVA*, *TfR-OVA-I*, *TfR-OVA-II*, and *mCiita* and *TfR-OVA* were named MC-38/mCiita, MC-38/OVA, MC-38/OVA-I, MC-38/OVA-II, and MC-38/OVA/mCiita, respectively. *hCIITA*-transfected MEL04 cell line was named MEL04/hCIITA.

Mouse *B2m*-deletion and human TCR-deletion using CRISPR/Cas9 technology

Mouse *B2m*-deleted MC-38 cell line and endogenous TCR-deleted Jurkat cells were generated using the CRISPR/Cas9 technology. Targeting guide RNA (gRNA) sequences (5'-TTCGGCTTCCCATTCTCCGG-3' for mouse *B2m*, 5'-CTCGACCAGCTTGACATCAC-3' for human *TCRA*, and 5'-AGAAGGTGGCCGAGACCCTC-3' for human *TCRB*) were used for editing the genomic locus. The gRNA and Cas9 protein (Thermo Fisher Scientific) were transduced into MC-38 cells or Jurkat cells using the electroporation machine (BIORAD Catalog# 1652660J1). The expression was evaluated using flow cytometry.

B2m-deficient MC-38, MC-38/mCiita, and MC-38/OVA/mCiita cell lines were named MC-38/B2mKO, MC-38/B2mKO/mCiita, and MC-38/OVA/B2mKO/mCiita, respectively.

In vitro assays for human PBMCs

To evaluate PD-1 and CXCL13 expression in $CD8^+$ T cells, PBMCs from healthy donors were cultured with indicated concentrations of anti-CD3 mAb, 10 μg/mL anti-CD28 mAb, and 30 IU/mL IL-2 (PeproTech, Cranbury, NJ) for 48 h and were subjected to flow cytometry.

Gene expression analysis

$PD\text{-}1^+$ or $PD\text{-}1^-CD8^+$ T cells from stimulated PBMCs of healthy donors or TILs of MC-38/OVA tumors sorted using a FACSAria instrument in Central Research Laboratory, Okayama University Medical School were subjected to quantitative reverse transcription PCR using PrimeScript RT Master Mix (TaKaRa, Cat# RR036A) and TB Green Premix Ex Taq II (TaKaRa, Cat# RR820S) according to the manufacturer's instructions. We used human *GAPDH* or mouse *Gapdh* as internal controls and calculated ΔC_t.

Luciferase reporter assay for cancer specificity

The endogenous TCR-deleted Jurkat cells were transduced using a pGL4.30 [luc2P/NFAT-RE/Hygro] vector, and antibiotic selection was performed with 100 μg/mL hygromycin for at least 2 weeks; these cells were named NFAT-Jurkat cells. pMX-*hCD4* and each pMSCV-*hTCRB-hTCRA* vector were transduced into these selected cells (Figure S5A). Each TCR-transduced $CD4^+$ NFAT-Jurkat cells were co-cultured with MHC-II-expressing MEL04/hCIITA cells (Figure S5B). Twenty-four hours after co-culture, luciferase activity was analyzed using the Bright-Glo Luciferase Assay System (Promega) according to the manufacturer's instructions. We compared the data with those from experiments without MEL04/hCIITA cells for statistical analyses and calculated the fold change. TCRs (#1–4) were selected from skewed T_{FH}-like cytotoxic $CD4^+$ T cell clonotypes from the cytotoxic population, and TCRs (#5 and 6) were selected from skewed non-cytotoxic T_{FH} cell clonotypes from the non-cytotoxic population (Table S5). Control clonotype TCR #0 was selected from a minor $CD4^+$ T cell clone in the TME that was frequently found in MHC-matched Adaptive Biotechnologies public peripheral blood datasets.[39] *In vitro* experiments were performed in triplicate.

Killing assay

Killing assays were performed using calcein-AM (Thermo Fisher Science). Briefly, $PD\text{-}1^+CXCR3^+$, $PD\text{-}1^+CXCR5^+$, or $PD\text{-}1^-CD25^-CD4^+$ T cells were sorted from C57BL/6J or *OT-II* mouse splenocytes using FACSMelody or FACSAria in Central Research Laboratory, Okayama University Medical School. In addition, $LAG\text{-}3^+PD\text{-}1^+CXCR5^+$, $LAG\text{-}3^-PD\text{-}1^+CXCR5^+$, or $PD\text{-}1^-CD25^-CD4^+$ T cells were sorted from MC-38/mCiita tumors in *OT-II* mice 14 days after inoculation using FACSMelody or FACSAria in Central Research Laboratory, Okayama University Medical School. Calcein-AM-labelled MC-38/OVA/B2mKO/mCiita cells (target cells; T) were co-cultured with sorted T cells (effector cells; E) at the indicated E/T ratios and centrifuged to ensure contact between the cell populations. Furthermore, Calcein-AM-labeled MEL04/hCIITA cells (T) were co-cultured with TCR-transduced $CD4^+$ T cells (E) at the indicated E/T ratios and centrifuged to ensure contact between the cell populations. Fluorescence was measured after 3 h of incubation. *In vitro* experiments were performed in triplicate.

Ex vivo assays of T_{FH} cells

Sorted LAG-3$^+$PD-1$^+$CXCR5$^+$CD25$^-$CD4$^+$ T cells (LAG-3$^+$ T_{FH} cells) and LAG-3$^-$PD-1$^+$CXCR5$^+$CD25$^-$CD4$^+$ T cells (LAG-3$^-$ T_{FH} cells) from MC-38/mCiita tumors 14 days after inoculation were labelled with 0.5 μM CFSE for 5 min at 37°C. Both T_{FH} cells were cultured separately in the presence of 0.5 μg/mL anti-CD3 and 10 μg/mL anti-CD28 mAbs, and 30 IU/mL IL-2 (PeproTech). Proliferation was assessed 3 days later by dilution of CFSE-labelled cells with flow cytometry. Apoptosis was also evaluated by flow cytometry using PE Annexin V Apoptosis Detection Kit with 7-AAD (BioLegend) 3 days after the treatment with anti-CD3 and anti-CD28 mAbs according to the manufacturer's protocol. Furthermore, anti-PD-1 mAb (BioLegend) and/or anti-LAG-3 mAb (BioLegend) were added at a concentration of 10 μg/mL simultaneously with anti-CD3 and anti-CD28 mAbs. Twenty-four hours later, the cells were analyzed for cytotoxicity using flow cytometry. *Ex vivo* experiments were performed at least twice.

In vitro transduction and analyses for T_{FH} cells from mouse splenocytes

Splenocytes from C57BL/6J mice were expanded with 0.5 μg/mL anti-CD3, 10 μg/mL anti-CD28 mAbs, 30 IU/mL IL-2, and irradiated allo-splenocytes from Balb/c mice, into which each lentiviral vector was transduced 4 days after expansion, resulting in *mTcf7*-overexpression or *mPrdm1*-knockdown. These cells were stimulated with 1.0 μg/mL anti-CD3 and 10 μg/mL anti-CD28 mAbs for 6 h and analyzed with flow cytometry. *In vitro* experiments were performed in triplicates.

Mouse TCR sequencing and data analyses

PD-1$^+$CXCR5$^+$CD25$^-$CD4$^+$ T cells (T_{FH} cells) and the other CD25$^-$CD4$^+$ T cells (CD4$^+$ non-T_{FH} cells) were sorted from MC-38/mCiita tumors before anti-PD-1 mAb treatment on day 5 and after the treatment on day 14 using a FACSAria instrument in Central Research Laboratory, Okayama University Medical School. The extracted RNA was subjected to TCR sequencing using a SMARTer Mouse TCRa/b Profiling Kit (TaKaRa Bio), according to the manufacturer's instructions. TCR libraries were sequenced using a MiSeq instrument (Illumina) and a 2 × 300 bp paired-end kit. Reads were assembled and aligned to mouse VDJ reference genes using the MiXCR software with default parameters.[74]

Flow cytometry analysis

Cells were washed with phosphate-buffered saline (PBS) containing 2% FBS and subjected to staining with surface antibodies. The antibodies used in the FCM analyses are summarized in Key Resource Table. Intracellular staining was performed with specific antibodies and the FOXP3/Transcription Factor Staining Buffer Set (Thermo Fisher Scientific) according to the manufacturer's instructions. For intracellular cytokine staining, GolgiStop or GolgiPLUG reagent (BD Biosciences) was added for the last 4 h of culture. Samples were assessed using a BD FACSVerse or a BD FACSFortessa instrument (BD Biosciences) and the FlowJo software (BD Biosciences).[20] The staining antibodies were diluted following the manufacturer's instructions. When we used IFN-ɤ (PeproTech, 1000 IU/mL), the cells were treated for 48 h before analyses. Annexin V (Fisher Scientific) staining was performed after cell surface staining as per the manufacturer's instructions. The same gating strategy was used in all figures to identify T_{FH} cells.

QUANTIFICATION AND STATISTICAL ANALYSIS

GraphPad Prism 8 (GraphPad Software, San Diego, CA) and R version 4.0.2 (R Foundation for Statistical Computing, Vienna, Austria) were used for statistical analyses. Differential gene expression analysis on single-cell datasets was performed through the FindMarkers function of the Seurat R package using the Wilcoxon rank-sum test. The relations of continuous variables between or among groups were compared using a t test or one-way ANOVA, respectively. The relations between tumor volume curves were compared using two-way ANOVA. For multiple testing, a Bonferroni correction was employed. PFS and OS were defined as the time from the initiation of anti-PD-1 mAb until the first observation of disease progression or death from any cause and until death from any cause, respectively. Survival curves were analyzed using the Kaplan–Meier method and compared among groups using the log rank test. p values <0.05 were considered statistically significant. All statistical details are provided in the figure legends.